

Dynamics of Time-Filtered 500-mb Vorticity

by

Stephen H. Scolnik

B.A., Yale University (1968)

Submitted in Partial Fulfillment of the
Requirements for the Degree of Master of Science

at the

Massachusetts Institute of Technology

August, 1974

Signature of Author
Department of Meteorology, August 12, 1974

Certified by
Thesis Supervisor

Accepted by
Chairman,
Departmental Committee on Graduate Students

WITHDRAWN
FROM
AUG 28 1974
MASS. INST. TECH.
MIT LIBRARIES

DEDICATION

To Susan,
who learned that weather is composed of waves

Dynamics of Time-Filtered 500-mb Vorticity

by

Stephen H. Scolnik

Submitted to the Department of Meteorology on August 12, 1974
in partial fulfillment of the requirements for the degree of
Master of Science

ABSTRACT

A numerical band-pass filter is used to study the dynamics of medium frequency (15 to 60-day period) motions at the 500-mb level in the atmosphere for a 2-year period. Although the choice of band limits is somewhat arbitrary, it is shown by spectral analysis of 10 years of data at a few selected points that this frequency band accounts for 17-29% of the total variance of height, geostrophic wind, and vorticity at latitude 40N. A diagnostic budget is calculated for the 9 advection terms representing the contributions to the medium frequency vorticity tendency of the various non-linear interactions among the low, medium, and high frequency bands. The largest of these terms represents the advection of medium frequency vorticity by the low frequency wind. This term shows a mean correlation with the vorticity tendency of 0.3 in middle latitudes. High frequency eddy forcing also plays an important role in the medium frequency vorticity budget. The "divergence" term, calculated as a residual, shows a consistently large magnitude, indicating the importance of non-advective effects for this frequency band.

Thesis Supervisor: John A. Young

Title: Visiting Associate Professor of Meteorology

TABLE OF CONTENTS

Abstract	3
I. Introduction	5
II. General aspects of filtering	8
A. Filtering and spectral analysis	8
B. Principles of filtering	12
C. Numerical techniques	15
D. Applications of filtering	16
III. Time-filtered 500-mb flow	18
A. Data	18
B. Spectral analysis	19
C. Time filter	27
D. Application to vorticity equation	29
E. Results	37
IV. Conclusions	47
A. Summary	47
B. Suggestions for future research	51
Acknowledgments	52
Tables	53
List of Figures	57
References	88

I. Introduction

The purpose of the present study is to use the technique of numerical filtering to investigate the dynamics of medium frequency (15 to 60-day period) motions at 500 mb. In particular, it is desired to examine the degree to which vorticity changes on this time scale are influenced by the fluxes arising from the various non-linear interactions among the low, medium, and high frequency bands of the quasi-geostrophic motion field.

It is well known that the spectra of atmospheric variables are essentially continuous, with no clear spectral gaps providing convenient boundaries for distinguishing between separate bands. Hence, any splitting of the spectrum into low, medium, and high frequencies must be rather arbitrary. Nevertheless, it is possible on the basis of our synoptic experience to make some qualitative distinctions. The transient cyclones and anticyclones of the daily weather map, with their characteristic periods of several days, may be considered representative of the high frequency band. The anomaly patterns characteristic of 30-day mean charts may be considered representative of the medium frequency band. Finally, the slowly evolving seasonal and annual patterns may be considered representative of the low frequency band.

These distinctions are quite subjective, however. In order to assign particular cut-off periods to the boundaries of our medium frequency band, we must be more objective.

Clearly, we would like to eliminate transient synoptic-scale motions on the high-frequency end. Present daily forecasting procedures show positive skill at a range of at least 5 days, and Lorenz (1973) has shown that marginal predictability of daily patterns is likely to exist up to a range of 12 days. Beyond 15 days, such detailed predictability is unlikely to exist, however. Hence, a 15-day cut-off for the high-frequency end of the medium frequency band appears to be clearly beyond the range of synoptic-scale variability.

On the other end of the scale, we recognize that extended forecasting using mean circulation methods has shown positive, if meager, skill at forecasting 30-day patterns (Namias, 1953). Although seasonal (90-day) patterns may be closely related to 30-day patterns (indeed, a marginal degree of skill has been shown [Namias, 1964] in seasonal forecasting methods based on an extension of 30-day techniques), they may also be classed with the annual variations which we would definitely prefer to exclude from the medium frequency band. Thus, a cut-off period of 60 days appears reasonable, if somewhat less firmly based than our high-frequency cut-off.

In order to test whether there are indeed motions of interest within the 15 to 60-day period range, we may use spectral analysis to measure the variance distributions of height, geostrophic wind, and vorticity. If it appears that there is indeed sufficient variance within our chosen band to justify further consideration, we may proceed with the filtering process

to obtain more information about the dynamics of such motions. Since the medium frequency motions to be considered are generally of large scale and we shall be specifically interested in those of middle latitudes, we may use the quasi-geostrophic vorticity equation for this purpose. The methods and results of the analysis will be discussed in section III, after a consideration of the background of the filtering problem in section II.

II. General aspects of filtering

A. Filtering and spectral analysis

Atmospheric motions are composed of many different scales, both in space and in time. Numerical filtering provides a method of isolating particular scales of these motions for detailed study. Thus, filtering is a complement of spectral analysis, which is a tool for decomposing a given field into its components of various space and time scales.

Spectral analysis is based upon the fact that any continuous function which is bounded on a finite domain may be represented by a series of orthogonal functions. In meteorology, we are concerned with functions of the form $f(x,y,z,t)$ where x , y , and z represent spatial distances and t represents time. If f is now expanded in terms of a series of orthogonal functions, each term in the series represents a particular scale of the variation of the field of f , and the square of the coefficient of the term represents a measure of the magnitude of that variation. The set of such squares of coefficients is called the spectrum of f . Spectral analysis has been found to be particularly useful in general circulation studies, in which such methods have been used to determine the spatial scales of motion which are most important in maintaining the time-averaged state of the atmosphere. Spectral studies are also significant in the problem of atmospheric predictability. Lorenz (1969), for example, has shown that the shape of the spectrum

is important in determining the rate at which the "error energy" from imperfectly known smaller spatial scales of motion will contaminate a prediction of the larger scales.

The most general spatial representation of the atmospheric variables would be in terms of spherical harmonics. The amount of calculation required to represent a substantial collection of atmospheric data in terms of spherical harmonics is rather large, but such calculations have been carried out by Eliassen and Machenhauer (1965, 1969) and Deland (1965).

Since the larger scales of atmospheric motions tend to propagate more or less parallel to latitude circles, it has often been found convenient to express the dependent variables in terms of a Fourier series expansion in which longitude λ is the independent variable:

$$f(\lambda) = \sum_{k=-\infty}^{\infty} F(k) e^{ik\lambda} \quad (1)$$

The wavenumber k represents the number of waves of wavelength $2\pi/k$ which are contained in a latitude circle of length 2π . The derivation of the kinetic energy equations in the wavenumber domain was first presented by Saltzman (1957). Since that time numerous studies have used this formulation to investigate the atmospheric energy cycle. The most extensive such studies are those of Saltzman and Fleisher (1962), Saltzman and Teweles (1964), Horn and Bryson (1963), Julian et al. (1970), Wiin-Nielsen et al. (1964), Wiin-Nielsen (1967), and Yang (1967). These

investigations have shown that the spectrum of zonal velocity is characterized by a monotonic decrease with wavenumber, whereas the spectrum of meridional velocity shows a peak for cyclonic-scale motions (wavenumbers 4 to 6). Both spectra are approximately proportional to the -3 power of wavenumber in the range of wavenumbers larger than 8.

An equation analogous to (1) may be written using non-dimensionalized time t as the independent variable:

$$f(t) = \sum_{n=-\infty}^{\infty} F(n) e^{2\pi i n t} \quad (2)$$

Here n is the frequency of motions of period $1/n$ occurring in the normalized time interval 0 to 1. Despite the formal analogy, however, frequency spectra are fundamentally different in nature from wavenumber spectra. This difference arises from the fact that there is no maximum period which may exist, whereas the finite size of the earth imposes a limit on wavelength.

Spectral studies in the frequency domain have been far less numerous than those in the wavenumber domain. The most notable of these are the studies of Van der Hoven (1957), Oort and Taylor (1969), Kao and Bullock (1964), and Kao (1965). The kinetic energy spectra in the frequency domain have been found to be similar to those in the wavenumber domain, except that the spectrum of meridional velocity fails to show a peak for cyclonic-scale motions (Julian, 1971). Furthermore, the exponent in the power-law relationship for high frequencies (greater

than 1/(5 days)) is estimated to be around -2, as opposed to -3.

B. Principles of filtering

Although spectral analysis provides a useful method for determining the statistics of atmospheric motions, an investigation of the detailed dynamics of these motions using spectral decomposition can become computationally prohibitive if the number of wavenumbers or frequencies considered is at all large. This occurs because the non-linearity of the equations of motion introduces numerous cross-product terms when two Fourier series are multiplied together. The number of cross-products, or interaction terms, can become unmanageable unless some form of truncation of the series is used.

A filter is simply a systematic method of truncating the Fourier series representation of a function. As an example, we may consider the representation in the frequency domain given by (2). In practice, if the value of f is known at a finite number of times $2N$, then the maximum non-dimensional frequency which can be resolved by the data is N , which is called the Nyquist frequency. (If t is dimensionalized by multiplying by $\tau = 2N\Delta t$, then n must be divided by τ , and the dimensional Nyquist frequency becomes $N/(2N\Delta t) = 1/(2\Delta t)$, where Δt is the dimensional time interval between data values.) Hence, (2) becomes

$$f(t) = \sum_{n=-N}^N F(n) e^{2\pi i n t} = \sum_{|n| \leq N} F(n) e^{2\pi i n t} \quad (3)$$

A perfect filter would have the property of selecting only

a certain range of frequencies in (3), while completely eliminating others. Thus, we may define the ideal filter $(\overline{\quad})^L$ so that

$$\overline{f(t)}^L = \sum_{|n|=0}^L F(n) e^{2\pi i n t} \quad (4)$$

where L is some frequency less than N . This filter is called a low-pass filter since it preserves only those frequencies lower than the cut-off frequency L . The response function $R(n)$ may be defined for each frequency n as the ratio of the Fourier coefficient $F(n)$ of the filtered series to that of the corresponding term of the unfiltered series. Clearly, in this case

$$R(n) = 1 \text{ for all } n \leq L$$

$$R(n) = 0 \text{ for all } n > L.$$

We may now define a new low-pass (or medium-pass) filter $(\overline{\quad})^M$:

$$\overline{f(t)}^M = \sum_{|n|=0}^M F(n) e^{2\pi i n t} \quad (5)$$

where $L < M < N$. If we subtract (4) from (5), we obtain

$$f_M(t) = \sum_{|n|=L+1}^M F(n) e^{2\pi i n t} \quad (6)$$

The operator $(\overline{\quad})_M$ is called a band-pass filter, since it preserves those frequencies in the band from $(L+1)$ to M . Finally,

we may subtract (5) from the original series (3) to obtain

$$f_H(t) = \sum_{|n|=M+1}^N F(n) e^{2\pi i n t} \quad (7)$$

The operator $(\)_H$ is a high-pass filter, since it selects those frequencies higher than M . Now, we may write

$$f(t) = f_L(t) + f_M(t) + f_H(t) \quad (8)$$

where $f_L(t) = \overline{f(t)}^L$. The function f has been separated into three components, each of which represents a particular frequency band. In later applications, we shall focus particular attention on the medium frequency component f_M .

C. Numerical techniques

In practice, filtering is accomplished by the use of a weighting function $w(i)$ applied to the values of the function f at the discrete points t_k, t_{k+1}, \dots so that

$$\overline{f}(t_k) = \sum_{i=-m}^m w(i) f(t_{k+i}) \quad (9)$$

A commonly used filter is the equally-weighted running mean over the interval of $(2m + 1)$ values, for which

$$w(i) = \frac{1}{2m+1} \cdot \quad (10)$$

The response function $R(n)$ of this filter is approximately

$$R(n) = \frac{\sin \pi n T}{\pi n T} \quad (11)$$

where T is the interval $2m\Delta t$ and $\Delta t = t_{k+1} - t_k$ is the interval between successive values of f (Holloway, 1958). This response function has a rather broad cut-off, and it is even substantially negative for frequencies between $1/T$ and $2/T$. For frequency $3/(2T)$, the response is $-2/(3\pi) \approx -0.21$. By proper selection of the weights $w(i)$, however, filters with better response characteristics may be designed. The response function of the particular filter to be used in this study will be described in a later section.

D. Applications of filtering

The techniques of extended forecasting by mean circulation methods depend heavily on the principle of filtering. A 5-day or 30-day mean contour chart is constructed by applying an equally weighted running mean to the time series of height at each grid point on the chart. In the case of a 5-day mean, for example, motions with a period of 5 days are completely removed, since in the notation of (11), $T = 5$ days and $R = 0$ for $n = 1/(5 \text{ days})$. Motions of shorter period are considerably reduced in amplitude, although as noted above there is a negative response for periods $2 \frac{1}{2}$ to 5 days, with a maximum negative response for frequency $3/(2T)$, or period $3 \frac{1}{3}$ days.

Despite the crudeness of the filter, however, mean charts have been found useful in isolating the anomaly centers which dominate the circulation pattern for extended periods of time. These features in turn can be related to the mean temperature and precipitation patterns, as described, for example, in the classical papers by Namias (1947, 1953).

Young and Sikdar (1973) used band-pass filters to decompose a series of satellite cloud pictures in the tropical Pacific into three components with periods centered at 4, 6, and 10 days. This procedure allowed the identification of periods of wavelike activity as opposed to irregular activity. For the identified periods of regular activity, latitude-time and longitude-time diagrams were used to determine characteristic wavelengths and propagation speeds.

Jenne et al. (1974) used filtering to construct a motion picture showing the relationship between wave patterns of periods shorter and longer than 15 days. Their movie clearly shows how the shorter period waves are often steered along by the larger scale, longer period waves. The longer period waves, however, are also evolving, both through their own internal dynamics and through interaction with the shorter period waves. It is that longer period evolution which provided the impetus for this study. In order to investigate the dynamics of extended period fluctuations, the 500-mb height field was decomposed into three frequency bands. The procedure used and the results obtained will be described in the next section.

III. Time-filtered 500-mb flow

A. Data

The basic data for the study consist of a 10-year series of twice-daily Northern Hemisphere 500-mb height analyses provided by the National Center for Atmospheric Research (NCAR). The data were interpolated from the 1977-point National Meteorological Center (NMC) grid to a 1009-point latitude-longitude grid extending from 20N to 90N at intervals of 5 degrees of latitude and longitude. The period of coverage extends from December 1, 1962 to December 31, 1972.

In order to obtain a measure of the frequency characteristics of the data to be studied, power spectra were calculated using the full period of record for height, u and v components of the geostrophic wind, and geostrophic vorticity at 6 points which were widely separated geographically. Then, the selected filtering function was applied to a 3-year series of height data. These filtered heights were used to evaluate the terms of the time-filtered quasi-geostrophic vorticity equation for the 2-year period from May 20, 1963 through May 19, 1965.

B. Spectral analysis

It is well known from previous studies that the spectrum of any atmospheric variable is essentially continuous beyond a period of one day, with no well-defined spectral gaps. For this reason, the selection of a cut-off frequency for a filtering function must be rather arbitrary. In fact, it has been suggested that the choice of 5-day and 30-day periods as the standard intervals in extended forecasting practice had little to do with the physical characteristics of the system being studied. Twice-daily maps over a period of 5 days yield a divisor of 10, which is obviously a great convenience when the averaging is done manually, as it was when extended forecasting procedures were first being developed. The choice of thirty days as a standard period is probably due largely to the influence of the calendar. Namias (1953) points out that all national meteorological services use the month as a standard data reporting interval.

Thus, it was considered useful to examine the power spectra of 500-mb height, geostrophic wind, and geostrophic vorticity for a selected number of widely separated points. Using the entire 10-year period of record, spectra were computed at each of the six selected points shown in table 1. The series of 7,368 values for each variable at each point was extended to 8,192 (2^{13}) values by using the mean value for that point to fill in the additional values. This was done in order to take advantage of the computational efficiency of the fast Fourier

transform method of spectrum estimation (Cooley and Tukey, 1965). After the Fourier transform of each time series was obtained, the sum of the squares of the sine and cosine coefficients was calculated for each frequency. This quantity is equal to the power density, or variance per unit bandwidth associated with that frequency. In order to improve the statistical reliability of the spectral estimates, values were averaged over bands of width 0.1 in units of \ln frequency. This split the 4096 raw spectral estimates into a total of 70 bands, with the number of values in each band ranging from 1 for the lowest frequencies to 364 for the highest frequencies. The resulting spectra were smoothed by applying a 3-point running mean to the band averages. This produced a further increase in the number of degrees of freedom of the spectral estimates. The smoothed power densities were normalized by dividing each value by the total variance for the complete spectrum. The normalized values were multiplied by frequency and plotted as a function of \ln frequency in figures 1 - 18. As Oort and Taylor (1969) point out, this is an equal area plot, since, denoting power density by P , total variance by V , and frequency by n ,

$$V = \frac{\int_{\ln n_1}^{\ln n_2} P \cdot n \, d(\ln n)}{\ln n_1} = \int_{n_1}^{n_2} P \, dn \quad (12)$$

The total height variance, shown in table 1, ranges from 1544 m^2 in the tropics to 32,694 m^2 over the central Pacific.

There is also considerable variation with longitude; the value of 9141 m^2 over central Asia is much lower than the central Pacific value at the same latitude. It is tempting to ascribe this longitudinal variation to differences in the circulation regimes imposed by oceans and continents. Caution must be used in this connection, however, since the large variance found over the central Pacific may be due at least partly to sparseness of data in the original analyses, rather than a true physical effect. In any case, the results are consistent with those of Lahey et al. (1958), which show that the month-by-month standard deviations of height based on 8 years of daily data are generally larger over the Pacific than over the continents.

The annual cycle is large at all of the points; it is largest over Asia (58.8% of total variance before smoothing) and smallest in the tropics (10.3% of total variance). The arctic point shows a distinct semi-annual peak (2.2% of total variance), much larger than that shown by any other point. A significant amount of variance is found in the medium frequency range associated with periods from 15 to 60 days. After removing the variance associated with the annual cycle, the percent of total variance accounted for by this band ranges from 22.8 over North America to 36.9 at 80N (table 2).

Many investigators have found that the spectra of atmospheric variables obey a power law of the form $P = an^b$ where P is power density, n is in the range of large wavenumber

(greater than about 8) or high frequency (greater than about $1/(5 \text{ days})$), and a and b are empirically determined constants. In general, a and b vary according to the particular type of spectrum being considered. For the kinetic energy spectrum in the wavenumber domain, turbulence theory (Charney, 1971) suggests a value of -3 for b , and this has been supported by the observational results (Horn and Bryson [1963], Wiin-Nielsen [1967], and Julian et al. [1970]). For frequency spectra, no such theory exists, but some attempts at the empirical determination of b have been made. Kao (1965) found a power-law relationship for the range of frequencies from $1/(5 \text{ days})$ to $3/(4 \text{ days})$. Kao and Wendell (1970) made a rough estimate of b without specifying the particular range to which it applied. Chiu (1973) considered the slope in the range from $1/(17 \text{ days})$ to $1/(2 \text{ days})$.

All of the present height spectra (figures 1 - 6) show a decrease of power with frequency in the high frequency range which is indicative of such a power-law relationship. To investigate this question, \ln power was plotted as a function of \ln frequency. An example of such a plot is shown in figure 19. Least squares analysis was used to fit regression lines in the range of \ln frequency from 6.8 (period 4.6 days) through 8.2 (period 1.1 days). The slopes obtained range from -1.66 in the tropics to -3.16 over North America (table 3). The goodness of fit was estimated by calculating correlation coefficients for each set of values. These ranged from $-.965$ to $-.997$.

Spectra were also computed for the zonal (u) and meridional (v) components of the geostrophic wind for the same six points (25N, 180E was substituted for point 5, since 20N was the boundary of the data region). These are shown in figures 7 - 12, using the same plotting system as was used for the height spectra. The Pacific point, which had the maximum total height variance, also had the maximum u variance and nearly the maximum v variance (table 1). The lowest total variances for u and v both occurred over Asia. Most points had greater u variance than v variance, although North America and the Arctic were both exceptions. All of the u spectra showed a much smaller annual cycle than the height spectra, except over the tropics. The v spectra in turn showed a consistently smaller annual cycle than the u spectra. The v spectra showed more relative power at higher frequencies than the u spectra, except for point 6 (80N), where there was little difference in the basic shape of the two spectra. The u spectra in turn showed larger relative power than the height spectra at medium and high frequencies, except for point 5 (25N).

In general, all of the wind spectra showed a decrease in power with increasing frequency. This "red noise" characteristic was also noted by Chiu (1973) and Julian (1971). The apparent maxima near $\ln \text{frequency} = 7.0$ (period approximately 4 days) on several of the v spectra should not be taken as an indication of a true spectral peak. Rather, they result from the particular method of analysis which has been used. When

the spectra are plotted as a function of linear frequency, these peaks are absent. The spectra for North America (40N, 100W) compare closely with Julian's v spectrum for Columbia, Mo. (39N, 92W) and Chiu's u and v spectra for Denver, Colo. (40N, 105W). It should be noted that Chiu's tentative indication of a possible peak in the v spectrum near a period of 5 days is not supported by the present results. Indeed, the variance of point 2 is monotonically decreasing over the entire range from a period of 11.2 days all the way to the Nyquist period of 1.0 days, except for the apparent effects of aliasing which produce a slight increase for the last value.

In order to examine the spectral shape for high frequencies, \ln power was plotted as a function of \ln frequency (see figure 20 for an example). Slopes of the regression lines ranged from -1.68 over the tropics to -2.44 over North America for the u spectra, and from -1.38 over Asia to -2.60 over North America for the v spectra (table 3). These values may be compared with a value of -2 obtained by Kao (1965) for the spectrum based on Lagrangian velocities at 300 mb. Kao and Wendell (1970) found the slope to range from around -1 in low latitudes to -2 in high latitudes. Chiu (1973) found a range of slopes from $-3/4$ to $-6/5$ for the u spectra and from -0.58 to -1.13 for the v spectra. Chiu's estimates covered a much larger range of frequency, however. His values extended as low as a period of 17 days, but it is clear that there is a definite break in the slope of the spectra somewhere around \ln frequency = 6.8 (period

4.6 days). Thus, Chiu's values represent an average over an interval including segments with significantly different slopes.

The wind spectrum provides a picture of the time variation of velocity at a given point, but it yields no information about the spatial structure of that variation. Therefore, vorticity spectra were computed for the same points, using a 5-point finite difference representation to calculate the Laplacian of the height. These spectra are shown in figures 13 - 18. Once again the largest total variance was found over the Pacific, with the smallest over Asia (table 1). The vorticity spectrum for each point is generally similar to the corresponding v spectrum, but there is greater relative power for shorter periods, especially those less than 3 days, for which all of the vorticity spectra are larger. For the medium frequency range (periods 15-60 days), all of the mid-latitude points show a fraction of total variance less than 20%, although this percentage becomes 33% for the high and low latitude points. The shift toward the high frequency end of the spectrum in middle latitudes is well illustrated by point 1, which shows 33% of the total variance being accounted for by periods less than 3.4 days. Indeed, 68% of the total variance at point 1 is accounted for by motions with periods less than 15 days. Despite the general shift toward higher frequencies, however, three of the vorticity spectra show a larger annual cycle than the corresponding v spectra.

The vorticity spectra are generally characterized by "red noise", although there is a small relative maximum of power near the period of 30 days for all of the spectra, except at point 4, where this "peak" is found near a period of 41 days. (This is not clear on the plots shown, but it may be seen on a plot of power density vs. linear frequency.) There is no indication of such a maximum in the synoptic-scale region, where all of the spectra are monotonically decreasing except for minor fluctuations.

Slopes of the spectra in the high frequency region were rather consistent, ranging from -0.84 at 25N to -1.51 over North America (table 3). These values may be compared with the value of -1 obtained by Steinberg et al. (1971) using 3 months of data in the wavenumber domain. No comparable vorticity spectra for the frequency domain are known to exist in the literature.

C. Time filter

For the points studied, the range of period from 15 to 60 days accounts for about 20 - 40% of the total variance of height, winds, and vorticity (table 2). Hence, it was decided that there was sufficient justification to focus further attention on this medium frequency band. In particular, it was desired to investigate the degree to which vorticity changes within the band may be attributable to wave interactions within the band itself, as opposed to the fluxes arising from various other interactions within the higher and lower bands, and between pairs of different bands.

The filter chosen for the calculations was the 17-point weighting function used by Jenne et al. (1974). The weights for this function are listed in table 4, and the response function is depicted in figure 22 for two different cut-off frequencies. In general, the filter has a half-power point (amplitude = $1/\sqrt{2}$) for a frequency equal to $1/(7.5\Delta t)$, where Δt is the time interval between successive data values. The period $7.5\Delta t$ may be defined as the cut-off period of the filter. Thus, the cut-off period is 15 days for $\Delta t = 2$ days, and it is 60 days for $\Delta t = 8$ days. We may obtain the 2-day sampling interval by block-averaging groups of 4 successive twice-daily maps from the original data set. When the 17-point weighting function is applied, a 15-day cut-off period results. Similarly, the maps resulting from this medium-pass filter may be block-averaged again in groups of 4 to obtain an 8-day sampling

interval, with a 60-day cut-off resulting when the 17-point weighting function is reapplied. If this filtering process had perfect response characteristics, the result of the first filter would be the function \overline{f}^M of equation (5) and the result of the second filter would be \overline{f}^L of equation (4). In reality, figure 22 shows that there is not an immediate drop from response 1 to response 0 at the cut-off period. Thus, when we calculate the components f_L , f_M , and f_H :

$$\begin{aligned}
 f_L(t) &= \overline{f}^L(t) \\
 f_M(t) &= \overline{f}^M(t) - \overline{f}^L(t) \\
 f_H(t) &= f(t) - \overline{f}^M(t)
 \end{aligned}
 \tag{13}$$

they will not represent completely independent frequency bands. Nevertheless, the total field will still be identically equal to the sum of the components f_L , f_M , and f_H .

D. Application to vorticity equation

The quasi-geostrophic vorticity equation for frictionless flow on a mid-latitude beta plane may be written (Holton, 1972):

$$\frac{\partial \zeta_g}{\partial t} = -\vec{v}_g \cdot \nabla(\zeta_g + f) - f_0 \nabla \cdot \vec{v} \quad (14)$$

where ζ_g is the geostrophic vorticity $\nabla^2 \phi / f_0$, \vec{v}_g is the geostrophic velocity $\hat{k} \times \nabla \phi / f_0$, f is the Coriolis parameter $2\Omega \sin \phi$, f_0 is a constant value of f , and \vec{v} is the total horizontal velocity. Since $\nabla \cdot \vec{v}_g \equiv 0$, we may write (14) in flux form:

$$\frac{\partial \zeta_g}{\partial t} = -\nabla \cdot \vec{v}_g (\zeta_g + f) - f_0 \nabla \cdot \vec{v} \quad (15)$$

Introducing the approximation $f = f_0 + \beta y$, we obtain

$$\frac{\partial \zeta_g}{\partial t} = -\nabla \cdot (\vec{v}_g \zeta_g) - \beta v_g - f_0 \nabla \cdot \vec{v} \quad (16)$$

In order to evaluate this equation for ζ_M , the medium frequency component of ζ_g , we must consider the effect of filtering on the non-linear first term on the right. Let us examine the simple prototype non-linear equation

$$\frac{\partial A}{\partial t} = BC \quad (17)$$

Resolving A, B, and C into high (H), medium (M), and low (L) frequency components, we obtain:

$$\begin{aligned} \frac{\partial}{\partial t} (A_H + A_M + A_L) &= (B_H C_H + B_H C_M + B_H C_L) \\ &+ (B_M C_H + B_M C_M + B_M C_L) \\ &+ (B_L C_H + B_L C_M + B_L C_L) \end{aligned} \quad (18)$$

Applying the medium-pass filter ($\bar{\quad}^M$),

$$\begin{aligned} \frac{\partial A_M}{\partial t} + \frac{\partial A_L}{\partial t} &= \bar{B}_H C_H^M + \bar{B}_H C_M^M + \bar{B}_H C_L^M \\ &+ \bar{B}_M C_H^M + \bar{B}_M C_M^M + \bar{B}_M C_L^M \\ &+ \bar{B}_L C_H^M + \bar{B}_L C_M^M + \bar{B}_L C_L^M \end{aligned} \quad (19)$$

Applying the low-pass filter ($\bar{\quad}^L$) and subtracting,

$$\begin{aligned} \frac{\partial A_M}{\partial t} &= (\bar{B}_H C_H^M)_M + (\bar{B}_H C_M^M)_M + (\bar{B}_H C_L^M)_M \\ &+ (\bar{B}_M C_H^M)_M + (\bar{B}_M C_M^M)_M + (\bar{B}_M C_L^M)_M \\ &+ (\bar{B}_L C_H^M)_M + (\bar{B}_L C_M^M)_M + (\bar{B}_L C_L^M)_M \end{aligned} \quad (20)$$

where $(\bar{B}_H C_H^M)_M = \bar{B}_H C_H^M - \bar{B}_H C_H^L$, etc.

The terms along the diagonal from upper left to lower right in (20) represent contributions to $\partial A_M / \partial t$ arising from non-linear interactions within each of the three frequency bands, whereas the off-diagonal terms represent the contributions arising from non-linear interactions between pairs of different frequency bands. It is important to note in this connection that terms such as $\overline{B_H C_M^M}$ are not equal to zero, since the filter operator $(\overline{\quad})^M$ does not have the same effect as a simple averaging operator. To illustrate this point, we may apply the Fourier representations (6) and (7):

$$B_H C_M = \left(\sum_{|n|=M+1}^N b_n e^{2\pi i n t} \right) \left(\sum_{|m|=L+1}^M c_m e^{2\pi i m t} \right) \quad (21)$$

The resultant series contains terms of the form $d_\ell e^{2\pi i \ell t}$ where $1 \leq |\ell| \leq N + M$. Thus,

$$\overline{B_H C_M^M} = \sum_{|\ell|=1}^M d_\ell e^{2\pi i \ell t} \neq 0 \quad (22)$$

For a simple example in which there is no separation of scales, let

$$\begin{array}{ccc} \text{(L)} & \text{(M)} & \text{(H)} \\ B = b_1 \cos t + b_2 \cos 2t + b_3 \cos 3t & & \\ C = c_1 \cos t + c_2 \cos 2t + c_3 \cos 3t & & \end{array} \quad (23)$$

Then

$$\begin{aligned} B_H C_M &= b_3 \cos 3t \cdot c_2 \cos 2t \\ &= k \cos 3t \cdot \cos 2t \end{aligned} \quad (24)$$

where $k = b_3 c_2$.

Now,

$$\overline{B_H C_M}^M = \frac{k}{2} [\cos(3t+2t) + \cos(3t-2t)]^M = \frac{k}{2} \cos t \neq 0 \quad (25)$$

Thus, every possible pair of non-linear interactions may potentially contribute to $\partial A_M / \partial t$. The extent to which they do, however, will depend to some extent on the width of the frequency bands used. If $L \ll M$, then $(B_H C_L)_M$ may be small, since $(M + 1 - L)$, which is the lowest frequency arising from such an interaction, will be close to M , and thus there will be few interaction terms contributing to $(B_H C_L)_M$. Unless their magnitudes are large, the resultant contribution to the tendency $\partial A_M / \partial t$ will be small. When the interaction is between adjacent bands, on the other hand, the full range of frequencies is possible, unless there is a distinct spectral gap between the bands.

Returning now to the vorticity equation (16), we may apply the general result (20) to obtain the time-filtered vorticity equation:

$$\frac{\partial \zeta_M}{\partial t} = -\nabla \cdot (\vec{F}_{HH})_M - \nabla \cdot (\vec{F}_{HM})_M - \nabla \cdot (\vec{F}_{HL})_M$$

$$\begin{aligned}
& - \nabla \cdot (\vec{F}_{MH})_M - \nabla \cdot (\vec{F}_{MM})_M - \nabla \cdot (\vec{F}_{ML})_M \\
& - \nabla \cdot (\vec{F}_{LH})_M - \nabla \cdot (\vec{F}_{LM})_M - \nabla \cdot (\vec{F}_{LL})_M \\
& - \beta v_M - f_0 (\nabla \cdot \vec{V})_M
\end{aligned} \tag{26}$$

Here \vec{F}_{IJ} denotes the flux $\vec{V}_I \zeta_J$, where \vec{V}_I represents the I frequency band of \vec{V}_g and ζ_J represents the J frequency band of ζ_g . (The ∇ -operator is distributive over the time filter because of the linear character of the weighting function (9).)

As indicated in connection with (20), the terms $-\nabla \cdot (\vec{F}_{II})_M$ (denoted simply as II) represent the effect on the vorticity tendency $\partial \zeta_M / \partial t$ of interactions within the band I. The term $-\nabla \cdot (\vec{F}_{HH})_M$ (denoted HH), for example, represents the transfer up the scale from the high frequency eddies. This effect is analogous to the role of eddy forcing in driving the general circulation. The term $-\nabla \cdot (\vec{F}_{MM})_M$ (denoted MM) represents the effects of self-advection of the medium frequency eddies. In other words, this contribution to the vorticity tendency arises from the advection of the medium frequency vorticity field by the medium frequency wind itself. Finally, $-\nabla \cdot (\vec{F}_{LL})_M$ (denoted LL) represents a cascade down the scale from lower frequency motions. This term will make a significant contribution to the medium frequency band only through those frequencies L which are close to the cut-off frequency separating the two bands.

The terms $-\nabla \cdot (\vec{F}_{HL})_M$ (denoted HL) and $-\nabla \cdot (\vec{F}_{LH})_M$ (denoted LH), representing interactions between low and high frequencies, should be relatively small, since $L = 1/4M$ for the present filter. (This is because the cut-off frequency L is $1/(60 \text{ days})$, whereas the cut-off frequency M is $1/(15 \text{ days})$.) Thus, frequencies less than $3/4 M$ will not arise from these interactions.

The other four flux terms (LM, ML, MH, HM) represent interactions of the medium frequency band with each of the other two bands. The term LM may be visualized as the effect of advection of the medium frequency eddies by the larger scale low frequency wind. If the total flow were to consist of a medium frequency eddy pattern superimposed upon a constant basic current, then this would be the only advection term. On the other hand, if the low frequency field possesses spatial structure, then it may be advected by the medium frequency wind, thus contributing to the term ML.

The term MH represents a contribution to the medium frequency vorticity tendency arising from the advection of high frequency vorticity by the medium frequency wind. If there were a complete separation of scales, then this advection would affect only the high frequency tendency. Finally, the HM term arises from interaction of the high frequency wind with the structure of the medium frequency vorticity field.

The term $-\beta v_M$ represents the advection of earth vorticity and should be of the same order of magnitude as $\partial \zeta_M / \partial t$. The

divergence term depends on the non-geostrophic component of velocity and must therefore be found as a residual from all of the other terms if direct wind observations are not available.

The filter process outlined in Section C was applied to 3 years of twice-daily 500-mb height analyses extending from December 1, 1962 to November 30, 1965 to yield the low-frequency (H_L), medium-frequency (H_M) and high-frequency (H_H) components of the height field. Geostrophic winds (u and v components) were then calculated from each filtered height field using centered finite differences extending over 10 degrees of latitude and longitude. Vorticities were calculated from the height field using the 5-point finite difference form of the Laplacian operator. These winds and vorticities were then used to calculate terms in the time-filtered quasi-geostrophic vorticity equation (26) using the finite difference scheme in figure 23. The spatial derivatives were evaluated as follows: Using the height (h) values shown, u , v , and ζ were calculated at the points 1, 2, 3, and 4. (The subscript g denoting geostrophic quantities will be omitted here for simplicity.) The components (F_x , F_y) of the flux were calculated at the four points:

$$\begin{aligned} F_x &= u\zeta \\ F_y &= v\zeta \end{aligned} \tag{27}$$

Then the derivatives $\partial F_x / \partial x$ and $\partial F_y / \partial y$ were obtained at the

intermediate points and averaged in pairs to obtain a value of

$$D = \nabla \cdot (\vec{V}\zeta) \quad (28)$$

at the center of the grid square. In order to provide spatial consistency between this calculation of the flux terms and the calculation of $\partial\zeta_M/\partial t$, the vorticity tendency was evaluated at the four corner points and averaged to provide a value at the center of the square. A centered time difference with $\Delta t = 4$ days was used to calculate the tendency.

E. Results

The high, medium, and low frequency components of vorticity for the point 40N, 100W are shown in figure 24 for a 6-month period. The characteristic frequencies and amplitudes of the three components are clearly evident from the figure. The much larger amplitude of the high frequency component is quite consistent with the distribution of variance indicated by the spectrum for that point (low 7.9%, medium 15.1%, high 78% of total).

A longitude-time diagram of $\partial\zeta_M/\partial t$ along latitude 42 1/2N is shown in figure 25. The period covered extends from February 25, 1963 to February 14, 1964, with maps spaced at 2-day intervals. Considerable coherence in both space and time is shown in the figure. There is a definite tendency for a banded structure sloping toward the east with increasing time, indicative of an eastward propagating wave. Some of these patterns are remarkably persistent; the area of positive values which is centered near 20E on 3-29 can be followed eastward continuously all the way until it crosses longitude 0 and reappears at the left side of the diagram around 5-10. At this point, it joins with another positive area to the east which continues propagating eastward fully two-thirds of the way around the hemisphere again.

A significant region of apparent westward propagation begins around 8-10 and continues to 9-23, an interval of 44 days. This was the only such persistent westward propagating

feature, although shorter periods of westward propagation could be identified.

A total of 10 persistent areas of eastward propagation were identified for the purpose of estimating their propagation speed. The time intervals considered ranged upward from 18 days, although most were longer than 30 days; the maximum was 60 days. Speeds ranged from 2.8 to 12.5 deg day⁻¹, with the mean being 4.7. The speed of westward propagation of the region described above was 3.9 deg day⁻¹. There was little indication of a systematic variation in speed or longevity of propagation. Although the major period of westward propagation occurred in summer, there were also several periods of eastward propagation during the same season. In general, fall showed the least consistent propagation, with only one clearly identifiable case. It was this region which had the shortest lifetime (18 days) and the fastest speed (12.5 deg day⁻¹).

These results may be compared with those of Jenne et al. (1974), who studied the combined low and medium frequency fields (all periods greater than 15 days). They note that the total low-medium component shows an equal tendency for eastward and westward propagation. Thus, retrogression must be primarily due to the contribution of the low frequency component of the flow. On the basis of the present results, it seems fair to conclude that there is considerable persistence to the patterns of vorticity change associated with motions having periods between 15 and 60 days. In order to shed some light on

the dynamics involved in producing such changes, it is necessary to consider the flux terms on the right hand side of (26).

Clearly, a logical place to look for an explanation of the vorticity tendency pattern would be in the self-advection of the medium frequency flow field. However, a longitude-time diagram for the advection of medium frequency vorticity by the medium frequency wind $(-\nabla \cdot (\vec{F}_{MM})_M)$ in figure 25 shows much less organized banded structure. There is still some suggestion of eastward propagating waves in the tilt of the patterns, but estimates of the speed of this propagation indicated a range from 1.3 to 1.9 deg day⁻¹, much slower than that of the tendency patterns. Furthermore, there appears to be no clear relation between the phase of the flux and tendency patterns. Thus, the tendency is not directly dependent on the self-advection of the medium frequency pattern. Diagrams (not shown) of the other terms in the vorticity budget displayed a similar complexity. This is especially true for the high frequency eddy forcing $(-\nabla \cdot (\vec{F}_{HH})_M)$, which will be shown later to play a significant role in the vorticity budget. The general magnitude of many of the flux terms is higher than that of the tendency, indicating that there must be considerable cancellation among them. Thus, the medium frequency vorticity budget is a diagnostic, rather than a prognostic, relation.

In order to obtain a more detailed picture of the complex relationship among the various terms, they were all plotted as

a function of time at one particular point ($42\ 1/2N$, $97\ 1/2W$) for a one-year period. This time series is shown in figure 26. The dominance in amplitude of many of the flux terms (especially HM, MH, HH, and LM) vs. the tendency is clear from the figure.

Among the self-advection terms, the high frequency (HH) interactions generally show the largest amplitude, followed in order by the medium term (MM) and low term (LL). This implies that the flux of vorticity from the high frequency eddies into the medium frequency band is often larger than the contribution from the advection of medium frequency vorticity by the medium frequency patterns themselves. Thus, any theory which attempts to explain the dynamics of medium frequency motions purely on the basis of the medium frequency field would be ignoring a significant effect. Since the high frequency motions cannot be predicted in detail on the medium frequency time scale, the effects of high frequency eddy forcing must somehow be parameterized in order to construct a prediction model for the medium frequency band.

The two terms representing interactions between the medium and high frequency bands (MH and HM) often increase and decrease in amplitude together. For example, they are both relatively small from 6-19 to 10-5, and then they begin gradually larger oscillations which decrease again after about 11-30. They both achieve their maximum magnitude around 5-2, when they are nearly equal and opposite in sign. This tendency

toward cancellation appears to be often characteristic of the two terms. For example, they are almost exactly 180° out of phase from about 12-24 through 1-27.

The low-medium frequency interactions are clearly dominated by the LM term. This is graphically demonstrated by the "sum" curve representing their total contribution from 8-26 through 11-24. This makes sense physically, since LM represents the advection of medium frequency vorticity by the low frequency wind, and we should expect this to be larger than the interaction of the medium frequency wind with the structure of the low frequency vorticity field, which is relatively large scale in the first place. On the other hand, ML is certainly not trivial compared to the remaining terms; it is consistently larger in magnitude than the beta term, to which it is closely analogous. The two low-medium terms are often in phase for extended periods. A striking example of this occurs from 2-18 all the way through 5-24.

The final set of advection terms represent the effects of interaction between the high and low frequency bands. As explained earlier, these terms should be relatively small simply on the basis of the band limits chosen. This turns out to be particularly true for HL, which never exceeds an absolute value of 0.5, but LH manages to achieve a rather respectable amplitude during the periods 12-28 through 2-10 and 3-15 through 5-24. Here again, we would expect that it should be more likely that the low frequency winds steer the high frequency eddies, than that the high frequency winds steer the low frequency eddies. It is interesting to note that the two terms are very closely in phase from about 3-5 through 5-24, during which time the LM and ML terms were also found to be in phase.

The beta term at a given point is simply a constant times the v component of velocity. In this case, it is consistently larger in amplitude than the medium frequency vorticity tendency. The two terms are generally opposite in phase (note that $+\beta v_M$ is plotted).

The "divergence" term is calculated as a residual from all the other terms (tendency minus sum of advections and beta term). Thus, it includes all other physical effects which have been neglected in our statement of the vorticity equation. Furthermore, any numerical errors which have been introduced in the evaluation of the terms in the equation will also be reflected in this residual. Clearly, if this term were small, we could explain the vorticity tendency solely in terms of the advection balance. This is not the case, however. The implications of this situation for the medium frequency vorticity budget will be discussed in the conclusions.

In order to obtain a more general view of the qualitative conclusions obtained from this particular time series, various statistics were computed for each point of the grid array for a two-year period. The mean and standard deviation for each term in the vorticity budget, as well as its correlation with the vorticity tendency, were calculated. The mean values were found to be negligibly small for each term at all gridpoints. This is to be expected, since by definition the long term mean of a medium frequency quantity is zero.

The standard deviations, averaged along latitude circles, are shown in figure 27. They may be taken as a measure of the relative amplitudes of the terms. The amplitudes are generally largest in middle latitudes, although there is a sharp increase near the pole which is probably a reflection of the neglect of curvature in the finite-difference scheme. These mean amplitudes tend to confirm the qualitative conclusions drawn from the time series at an individual point. The high frequency self-advections are the largest of the single-band interactions, followed by the medium and low frequency terms. This is an important result, since it shows that high frequency eddy forcing plays a significant role in the medium frequency vorticity budget. Among the two-band interactions, the two low-medium terms are largest, followed by the high-medium and low-high terms. Comparing the two members of each pair with each other, we see that the term representing the steering of the higher frequency vorticity by the lower frequency wind is larger than the reverse steering in each case (i.e., $LM > ML$, $MH > HM$, $LH > HL$). The largest individual term is LM, representing the advection of medium frequency vorticity by the low frequency wind. This term is considerably larger than the tendency.

As was the case for the individual time series, the "divergence" term is also considerably larger than the tendency. The curve marked "total" represents the sum of all of the interaction terms for a six-month period; this is equivalent to

the medium frequency component of the total geostrophic vorticity advection. Its amplitude is roughly four times that of the tendency. This may be compared with a ratio of about 2 obtained by Clapp (1953) for the advection and tendency calculated using the barotropic vorticity equation on 5-day mean charts and a ratio of about 1.3 obtained in the early experiments (Staff Members, 1952) using the equation on twice-daily synoptic charts. Thus, it appears that as the period of the motions becomes longer, non-barotropic effects must increasingly compensate for the effects of vorticity advection.

The standard deviation is a measure of the amplitude of the flux associated with a given interaction term, but it does not measure the degree to which this flux is actually related to the observed vorticity tendency. Therefore, correlation coefficients were calculated at each gridpoint between the vorticity tendency and each of the terms on the right side of the vorticity equation. The zonally averaged correlation coefficients are shown in figure 28. The largest correlation for an individual term is shown by LH, which achieves a value of 0.3 around 50N. This is closely followed by LM, but LM is statistically a much larger term (standard deviation 2.2 at 50N vs. 0.5 for LH). Therefore, in the long run, LM must make a larger total contribution to the vorticity tendency.

The only other terms with distinct positive correlations are MM and ML. These are generally less than 0.1, however.

The largest negative correlation is found for the beta term, which is negative at every latitude. This is consistent with the observed eastward propagation of the medium frequency waves, since the effect of the beta term is to act in the direction of retrogression of the wave pattern. Generally negative, but small, correlations are found for ML and HL. The terms whose mean correlation coefficients never exceeded 0.1 in absolute value are not plotted. They include LL, HH, HM, and the "divergence" term. The fact that HH and the "divergence" are both relatively large and poorly correlated with the tendency poses considerable difficulty for any scheme to parameterize these effects.

For comparison purposes, the total medium frequency vorticity advection (sum of the 9 interaction terms) was correlated with the medium frequency vorticity tendency for a six-month period. This correlation, indicated by the "total" curve, exceeds that of LH south of 35N and from 45N to 57 1/2N, reaching a maximum value of 0.46.

Also shown is the "unfiltered" correlation, determined from the unfiltered vorticity advection and unfiltered tendency for twice-daily charts over a one-year period. The maximum value of about 0.63 for this relationship is clearly superior to that for the filtered data, indicating again the decline in importance of the vorticity advection in determining the tendency for longer period motions. It is interesting to note that this correlation is very close to the value of 0.69

obtained in some of the early attempts to use the barotropic vorticity equation as a synoptic forecasting tool (Staff Members, 1952).

IV. Conclusions

A. Summary

A numerical band-pass filter has been used to study the vorticity budget of medium frequency motions at the 500-mb level in the atmosphere. The medium frequency range has been defined somewhat arbitrarily to include motions with periods from 15 to 60 days. Nevertheless, this range may be identified qualitatively with the anomaly patterns typical of 30-day mean charts. The variance associated with the medium frequency band is about 26% of the total height spectrum at latitude 40N. This percentage is about 29% for the u component of geostrophic velocity, 23% for the v component, and 17% for the geostrophic vorticity. A longitude-time diagram at $42 \frac{1}{2}N$ indicates an eastward propagation on the order of 4.7 deg day^{-1} for the geostrophic vorticity tendency patterns.

The vorticity budget calculations for a two-year period show that many of the non-linear advection terms are larger in amplitude than the tendency itself, indicating that there must be a great deal of cancellation among them. Furthermore, the "divergence" calculated as a residual from the tendency and advection terms is rather large, indicating that other processes which have not been included are also significant. The largest amplitude interaction term is LM, representing the "steering" effect of advection of medium frequency vorticity by the low frequency wind. This term shows a mean correlation with the

vorticity tendency which is relatively large when compared with those of other terms, although it reaches a maximum of only 0.3 in middle latitudes. The LH term, representing the advection of high frequency vorticity by the low frequency wind, is also relatively highly correlated with the tendency, but it shows a much smaller amplitude than LM. The HH term, representing the self-advection of the high frequency motion field, has a large amplitude, indicating the importance of the high frequency eddy forcing in maintaining the medium frequency vorticity balance. No simple relationship exists between this eddy forcing and the resulting vorticity tendency, however.

In general, the advection is correlated with the tendency much less for medium frequency motions than for synoptic-scale motions. Even for the total medium frequency advection (sum of all interaction terms), the mean correlation coefficient at latitude $47 \frac{1}{2}N$ is 0.44 compared with 0.57 for the unfiltered advection. This, together with the size of the "divergence" term suggests that there may be other important physical processes which have been neglected. Furthermore, there may also be numerical errors introduced by the filtering technique.

Considering the numerical techniques first, we see that the successive filtering used to calculate the 9 individual interaction terms may be a source of error. However, the total advection $-\nabla \cdot (\vec{V}\zeta)_M$ calculated directly from unfiltered winds and vorticities was compared with the sum of the 9 terms

calculated separately, and it was found that the difference was generally on the order of a few percent. Thus, it seems reasonable that the terms as calculated are an accurate representation of the relative contributions of each interaction to the total advection.

Another source of numerical error is the fact that curvature has been neglected in the finite-difference scheme used to calculate the spatial derivative. This is probably a serious error close to the pole, as indicated by the large standard deviations found at very high latitudes, but is probably not very serious at lower latitudes. Finally, the spatial differencing introduces another error in the form of smoothing, which is an additional filtering effect. Insofar as the medium frequency motions are also of relatively large scale, they should not be seriously affected, however.

The physical effects which are neglected in the quasi-geostrophic vorticity equation include vertical advection of vorticity, non-geostrophic horizontal advection of vorticity, the twisting term, and friction. These are all included in the residual we have called "divergence". Non-advective effects are significant even for synoptic-scale motions; Lorenz (1974), for example, has found that the barotropic vorticity equation is less accurate, in the mean-square-error sense, than persistence in the prediction of synoptic-scale vorticity tendency. The results obtained here suggest that this would be even more true for the medium frequency range. Thus, while the present

results indicate the relative roles of various non-linear interactions in the advection budget, there are additional factors which must be considered in a full explanation of the vorticity balance. Because the medium frequency vorticity tendency is produced by the compensating interaction of a number of larger amplitude effects, no simple prognostic system may be used to predict the tendency. Through the use of a diagnostic system such as the one presented here, however, the relative magnitude of the various effects may be measured.

B. Suggestions for future research

In view of the relatively large amount of vorticity variance associated with motions of period less than 15 days, it would be worthwhile to do a similar vorticity budget calculation for a differently defined medium frequency band, perhaps including periods from 5 to 15 days. This period range accounts for 29% of the total vorticity variance at 40N, 100W, as opposed to 15% for the band studied. Presumably, the total advection of vorticity should be better correlated with the tendency for these relatively higher frequency motions, and the relationship among the various interactions would yield further insight into the role of advection in medium frequency motions.

An analysis of the influence of non-advective effects on the medium frequency vorticity tendency must at the very least include an estimate of the divergence. This could be done directly through the use of actual wind observations, or it could be done indirectly through the use of the omega equation and equation of continuity. This would require data at more than one level in order to evaluate the differential vorticity advection and $\partial\psi/\partial p$, as well as knowledge of the heating field, but it would be more accurate. The use of actual winds, on the other hand, would permit the evaluation of the non-geostrophic component of horizontal advection.

ACKNOWLEDGMENTS

Professor John A. Young suggested the topic, provided guidance throughout the course of the research, and carefully reviewed the manuscript. Professor Edward N. Lorenz also contributed helpful advice. The able and timely drafting of the figures was accomplished by Isabelle Kole. This research was supported by National Science Foundation Grant No.GA28203X2.

Table 1. Summary of spectral calculations

Data interval: December 1, 1962 to December 31, 1972

Location	Latitude	Longitude	Total variance			Vorticity (10^{-10}sec^{-2})
			Height (m^2)	u ($\text{m}^2 \text{sec}^{-2}$)	v ($\text{m}^2 \text{sec}^{-2}$)	
1. Pacific	40N	180E	32,694	164	113	12.0
2. North America	40N	100W	21,145	63	101	7.9
3. Atlantic	40N	40W	21,786	137	115	11.2
4. Asia	40N	80E	9,141	29	14	2.4
5. Tropics	20N*	180E	1,544	125	34	6.9
6. Arctic	80N	180E	29,837	51	103	6.3

* 25N for wind and vorticity spectra

Table 2. Variance of medium frequency band
 Variance 15.1-61.1 days as % of total*

Point	Height	u	v	Vorticity
1. Pacific	26.4	31.9	18.2	16.3
2. North America	22.8	26.3	24.8	15.1
3. Atlantic	32.3	32.4	23.8	20.3
4. Asia	23.2	26.7	25.2	17.9
5. Tropics	31.4	17.8	24.2	33.3
6. Arctic	36.9	41.0	45.8	33.0

* total less annual for height spectra

Table 3. Spectral shape for high frequencies (periods less than 4.6 days)

Point	Slope of ln power vs. ln frequency regression line			
	Height	u	v	Vorticity
1. Pacific	-2.49	-2.09	-2.32	-1.46
2. North America	-3.16	-2.44	-2.60	-1.51
3. Atlantic	-2.61	-2.19	-2.42	-1.50
4. Asia	-2.01	-1.88	-1.38	-0.94
5. Tropics	-1.66	-1.68	-1.82	-0.84
6. Arctic	-1.86	-2.07	-1.74	-1.46

Table 4. 17-point filter weighting function

w_0	=		.3200156553
w_{-1}	=	w_1	= .2643210644
w_{-2}	=	w_2	= .1343767864
w_{-3}	=	w_3	= .0114831529
w_{-4}	=	w_4	= -.0458900942
w_{-5}	=	w_5	= -.0377520979
w_{-6}	=	w_6	= -.0064753717
w_{-7}	=	w_7	= .0111929411
w_{-8}	=	w_8	= .0087357913

FIGURES

- 1-6. Spectra of 500-mb height variance for points listed in table 1. Abscissa is \ln frequency, where frequency is expressed in units of $(4096 \text{ days})^{-1}$. Ordinate is normalized power $\times 1000$. (Scale on left is 10 times scale on right.)
- 7-12. Spectra of u and v components of geostrophic wind.
- 13-18. Spectra of geostrophic vorticity.
19. \ln power as a function of \ln frequency for the high frequency range of the height spectrum at 40N, 100W. Least squares regression line indicated with slope m.
20. Same as 19, but for u component of geostrophic wind.
21. Same as 19, but for geostrophic vorticity.
22. Amplitude response function of 17-point filter for data intervals of 2 days (solid) and 9 days (dashed). Abscissa is linear frequency, labeled as equivalent period.
23. Finite difference grid used for vorticity budget calculations.
24. Time series of high, medium, and low frequency components of vorticity at 40N, 100W, in units of 10^{-5} sec^{-1} . (Scale for high frequencies is twice that for the other components.)
25. Longitude-time section along 42 1/2N for medium frequency geostrophic vorticity tendency (left) and self-advection of medium frequency vorticity (right).

- 25.(cont.) Positive values shaded.
26. a. Time series at 42 1/2N, 97 1/2W of advective components of medium frequency geostrophic vorticity tendency in units of $10^{-10} \text{ sec}^{-2}$.
- b. Time series at same point of vorticity tendency, beta term, and "divergence"
27. Zonally averaged values of standard deviation for vorticity budget terms in units of $10^{-10} \text{ sec}^{-2}$. (See text for notation.)
28. Zonally averaged values of correlation coefficient between vorticity tendency and terms of vorticity budget. (See text for notation.)

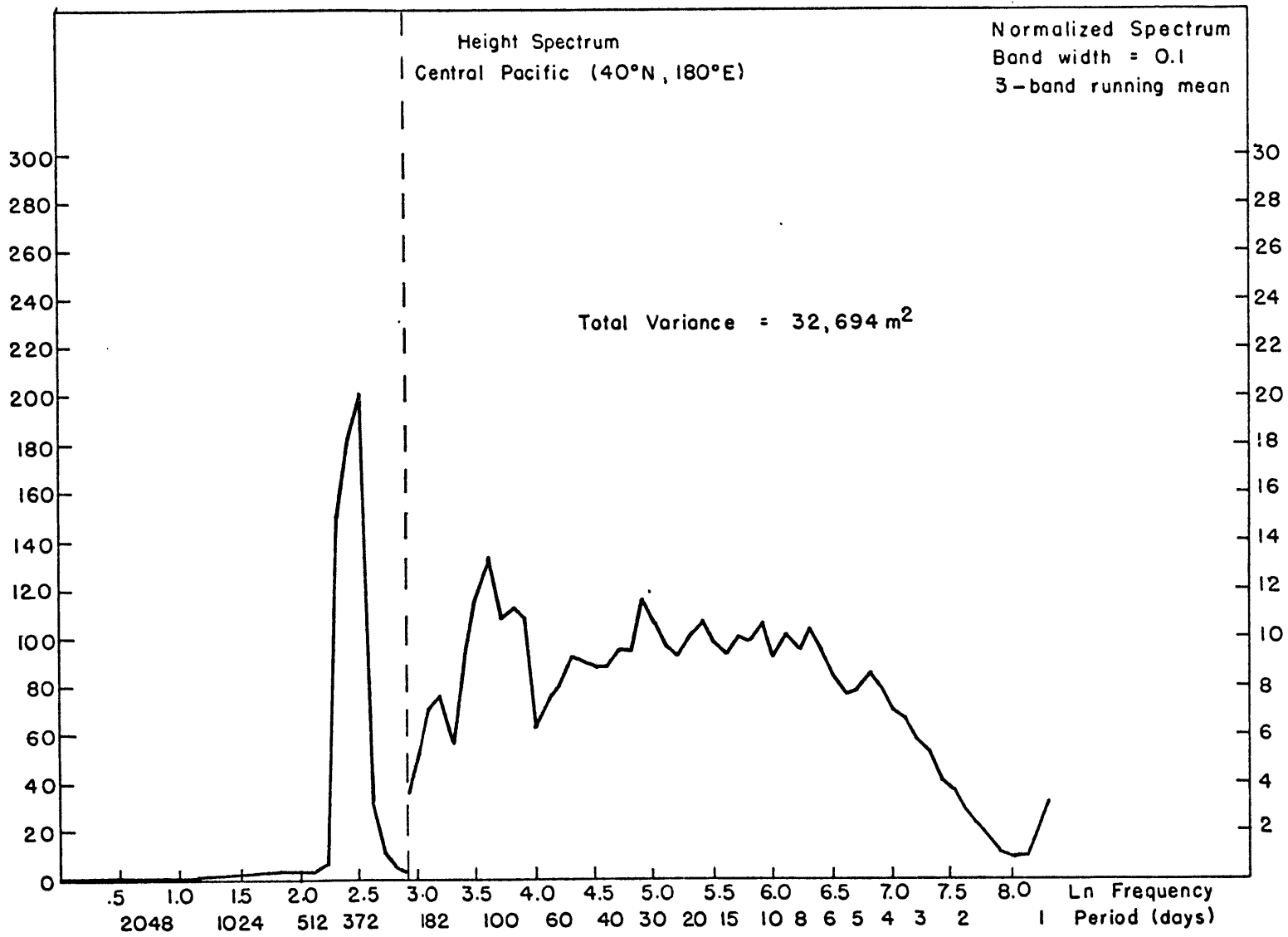


Figure 1.

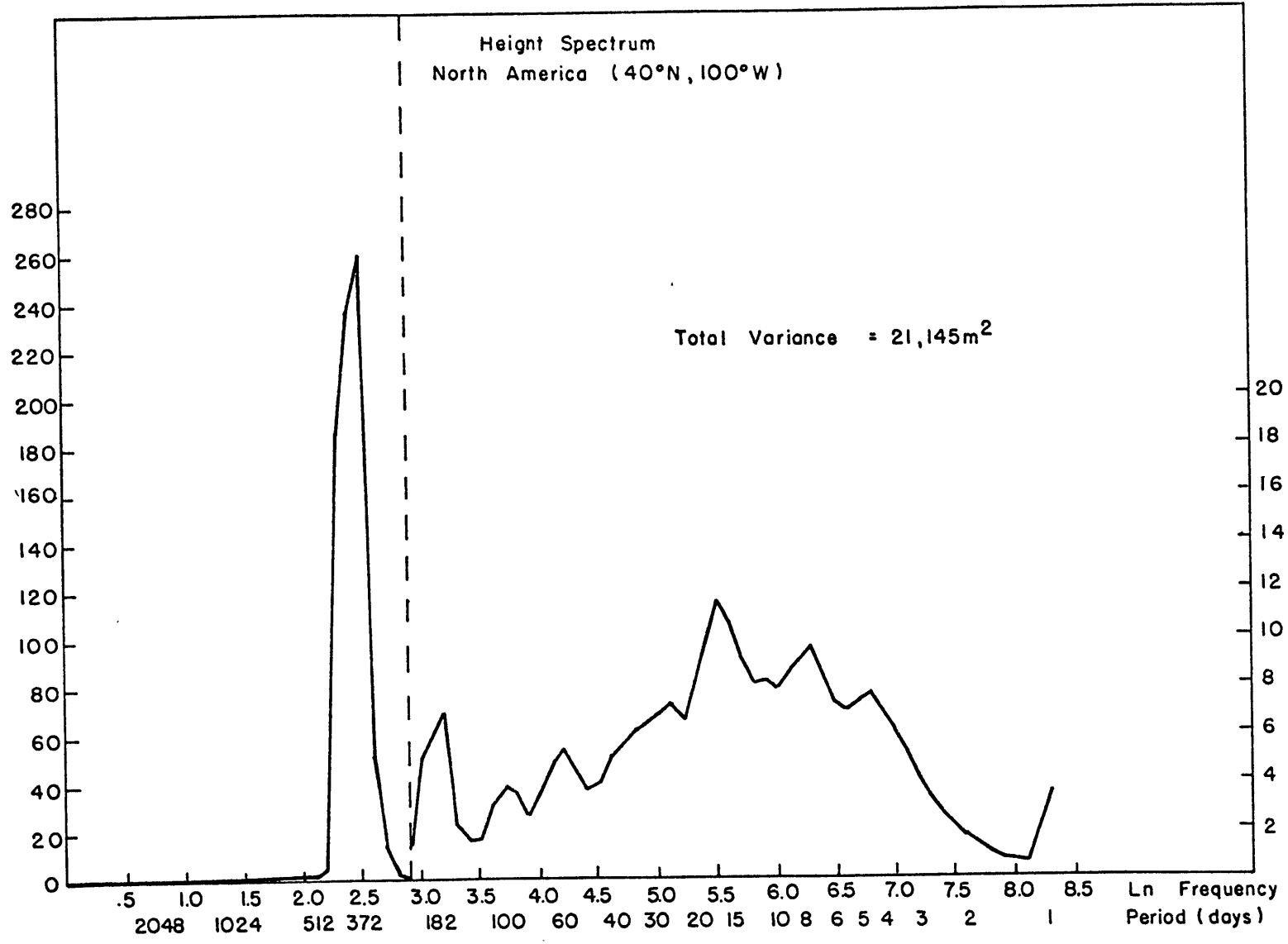


Figure 2.

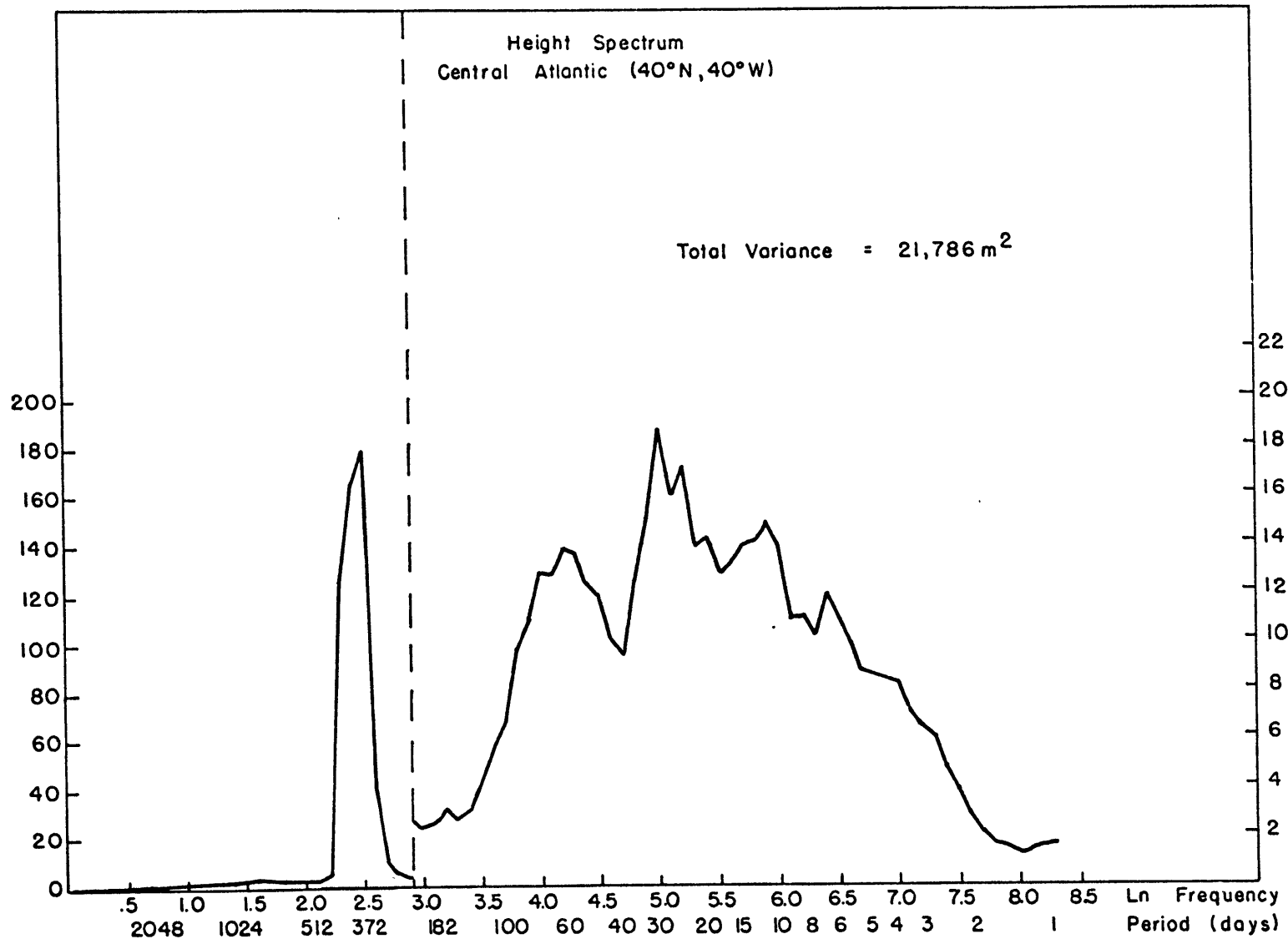


Figure 3.

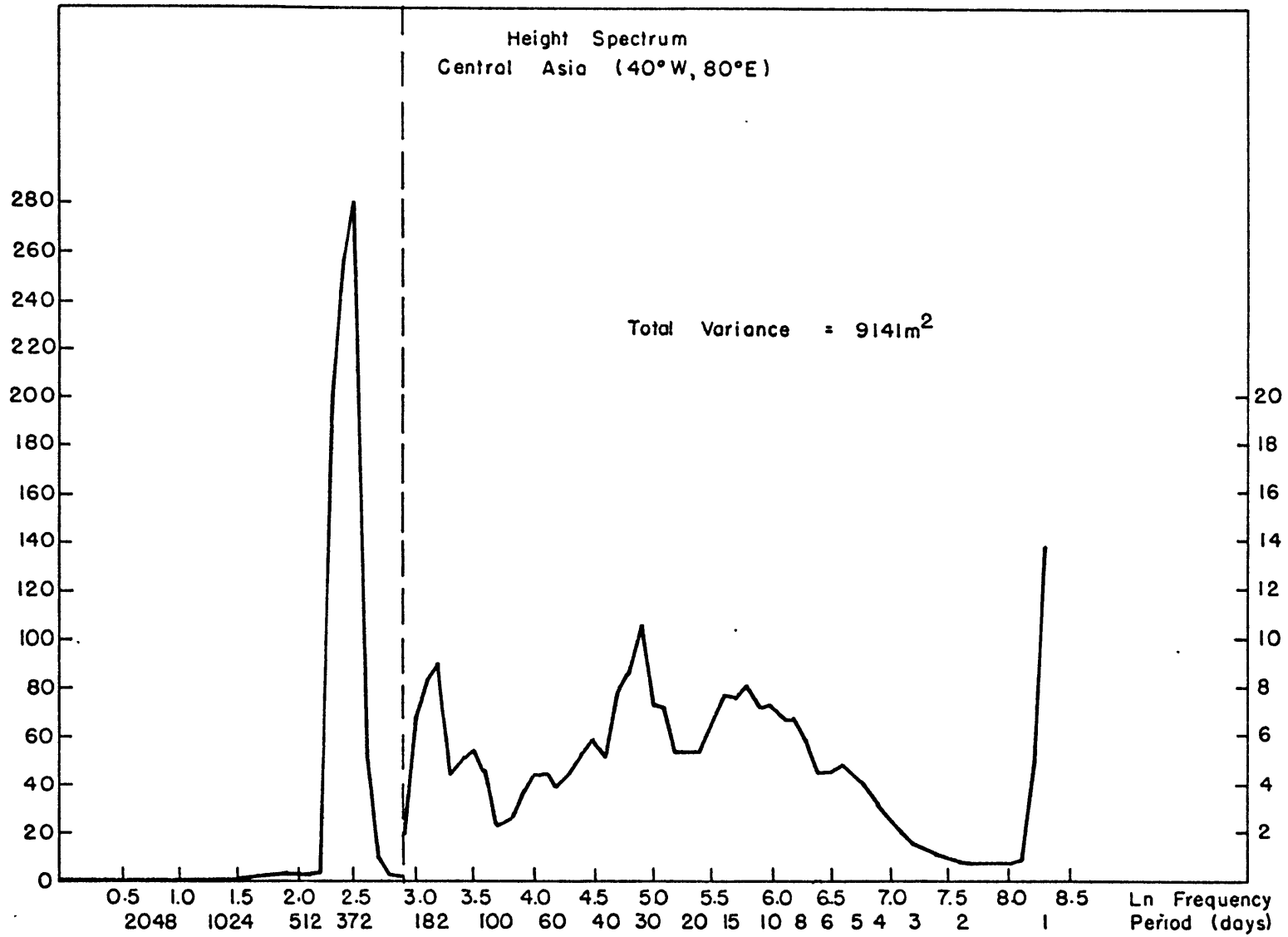


Figure 4.

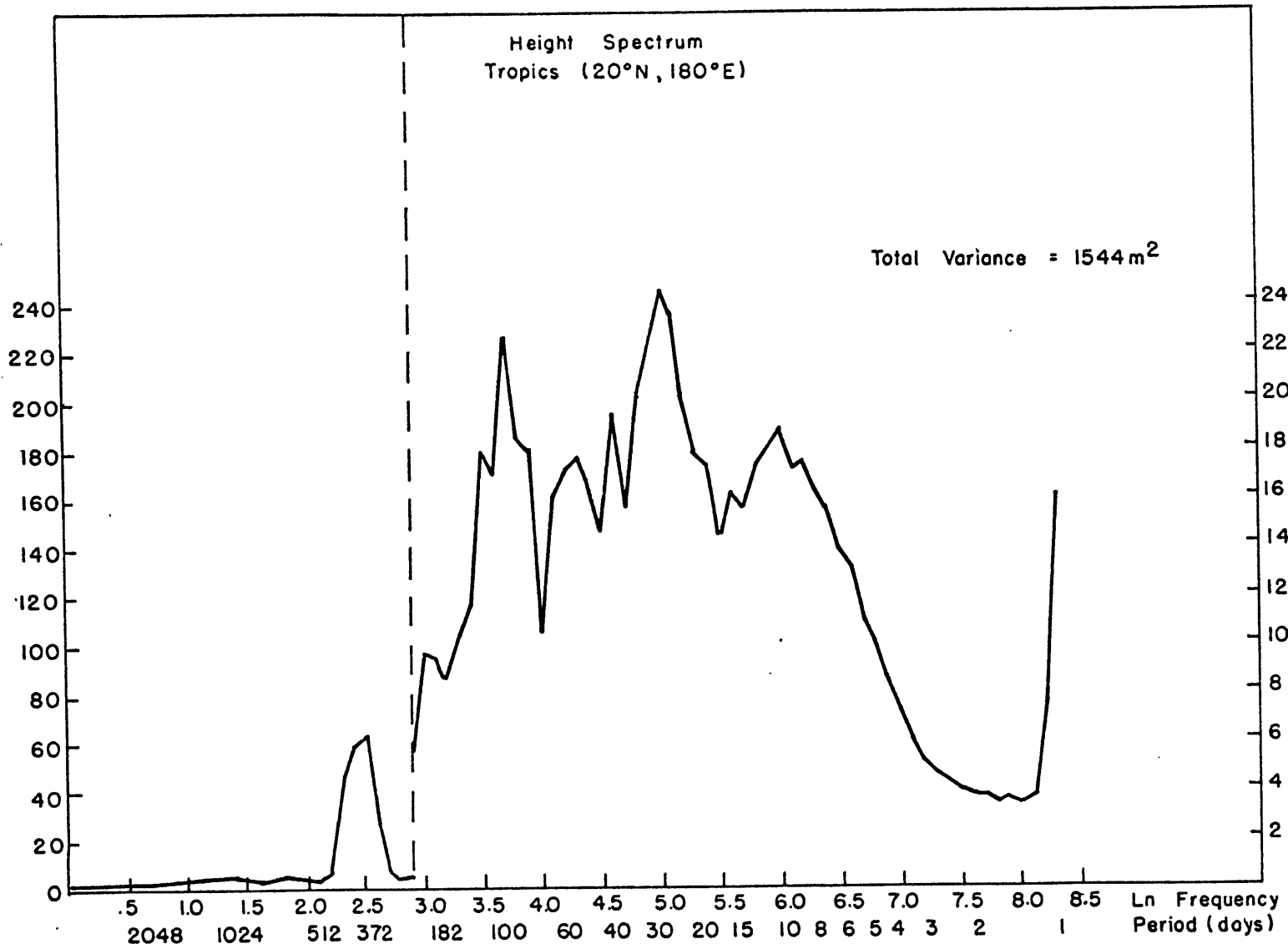


Figure 5.

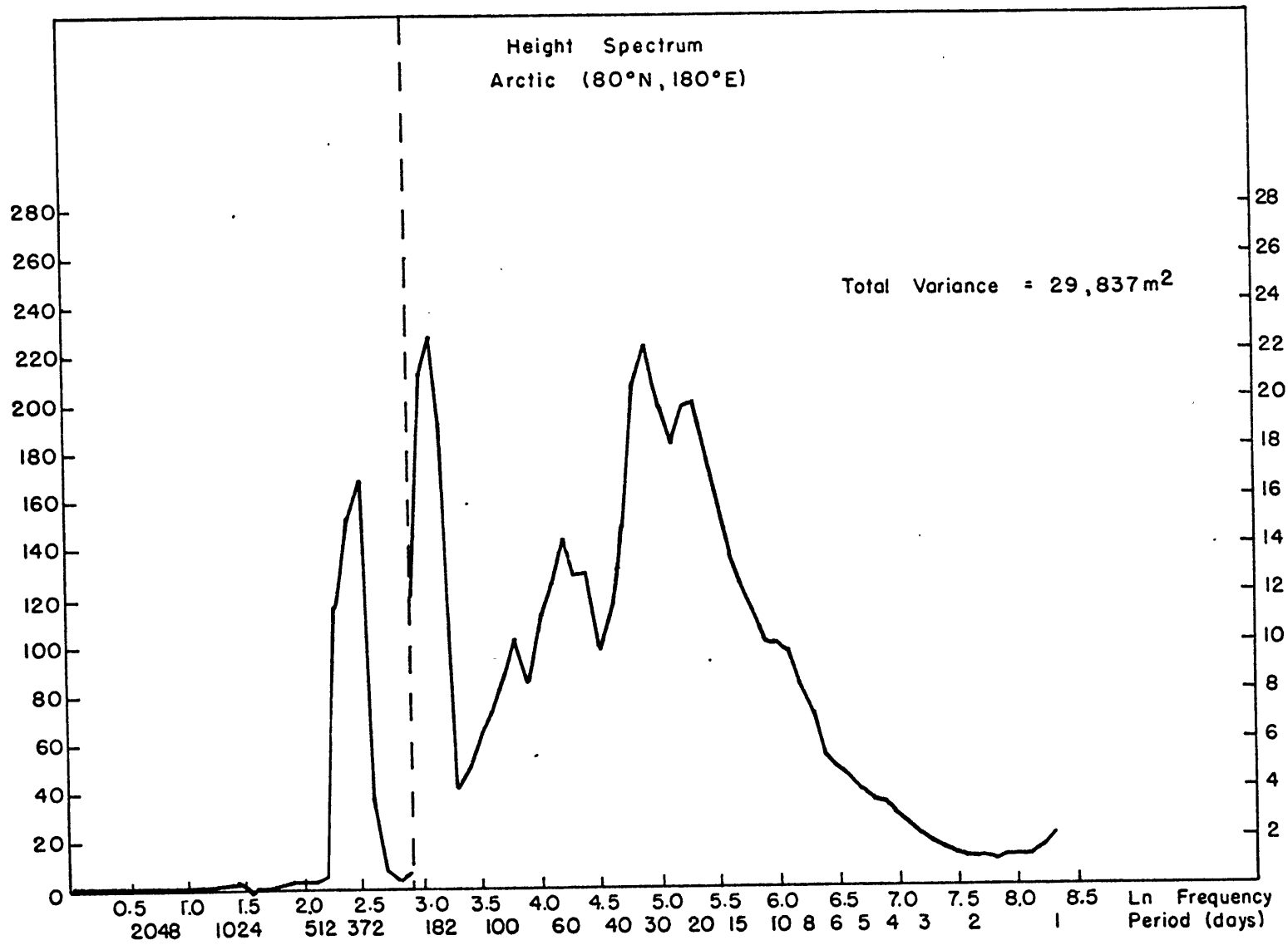


Figure 6.

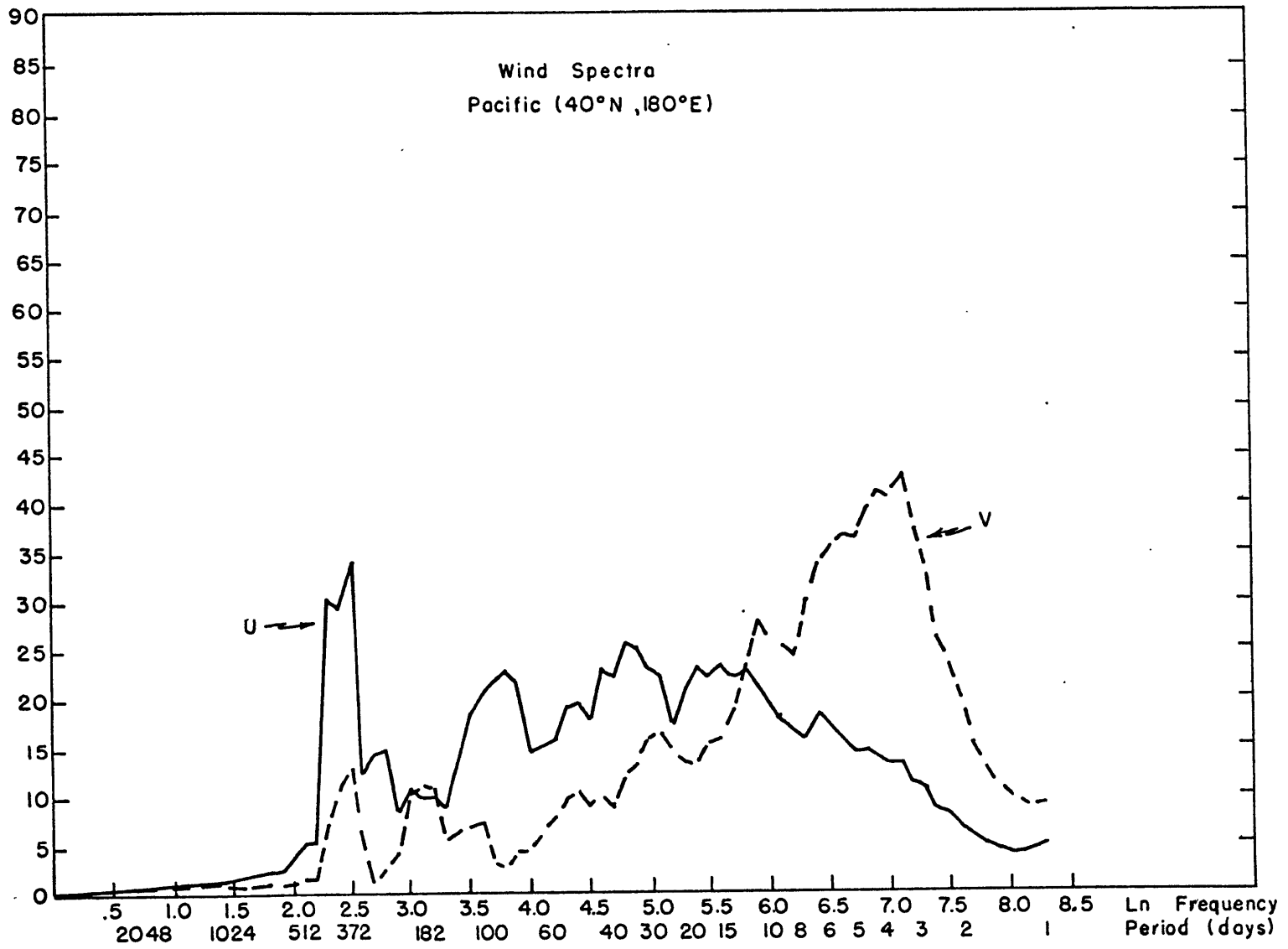


Figure 7.

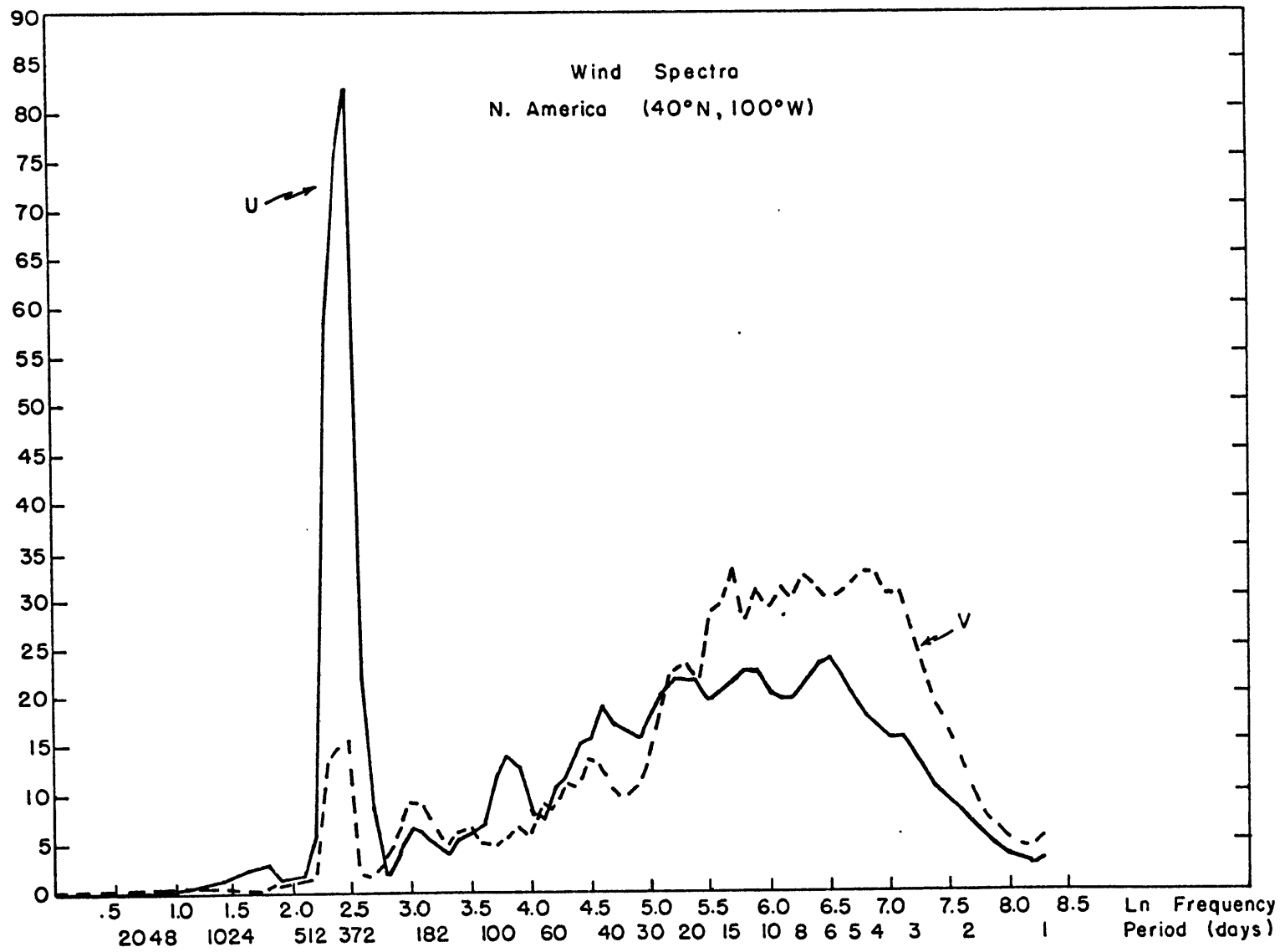


Figure 8.

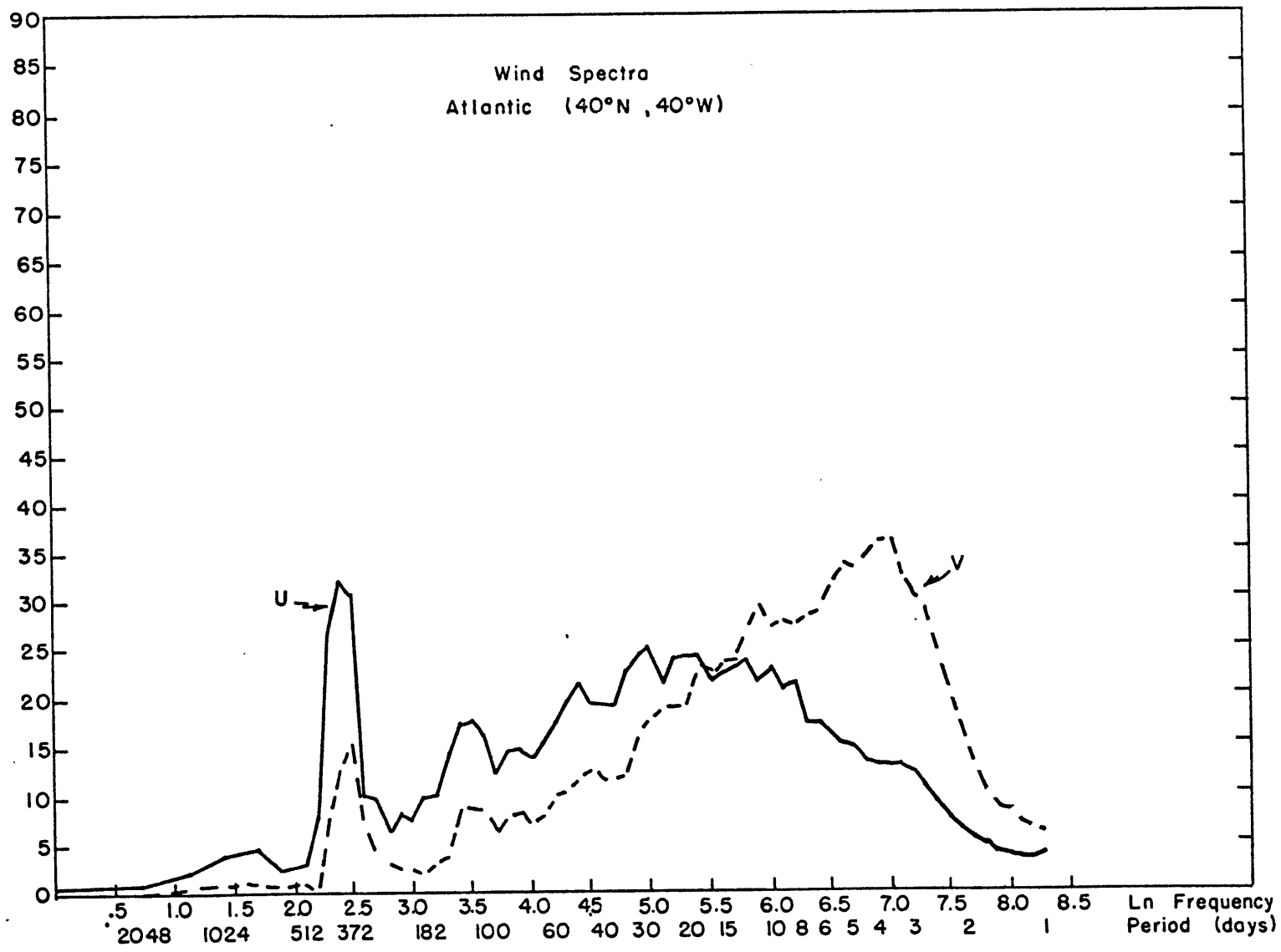


Figure 9.

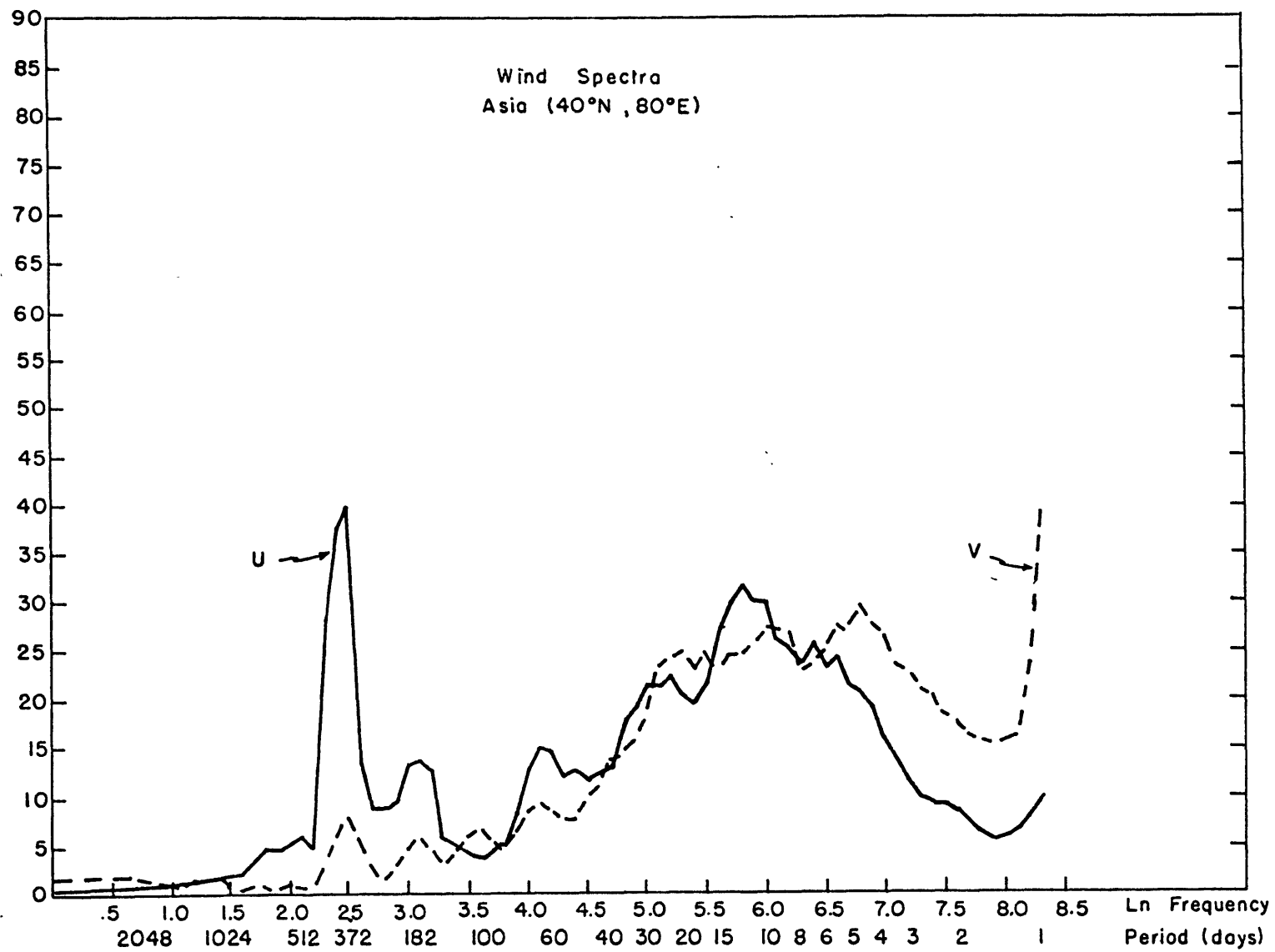


Figure 10.

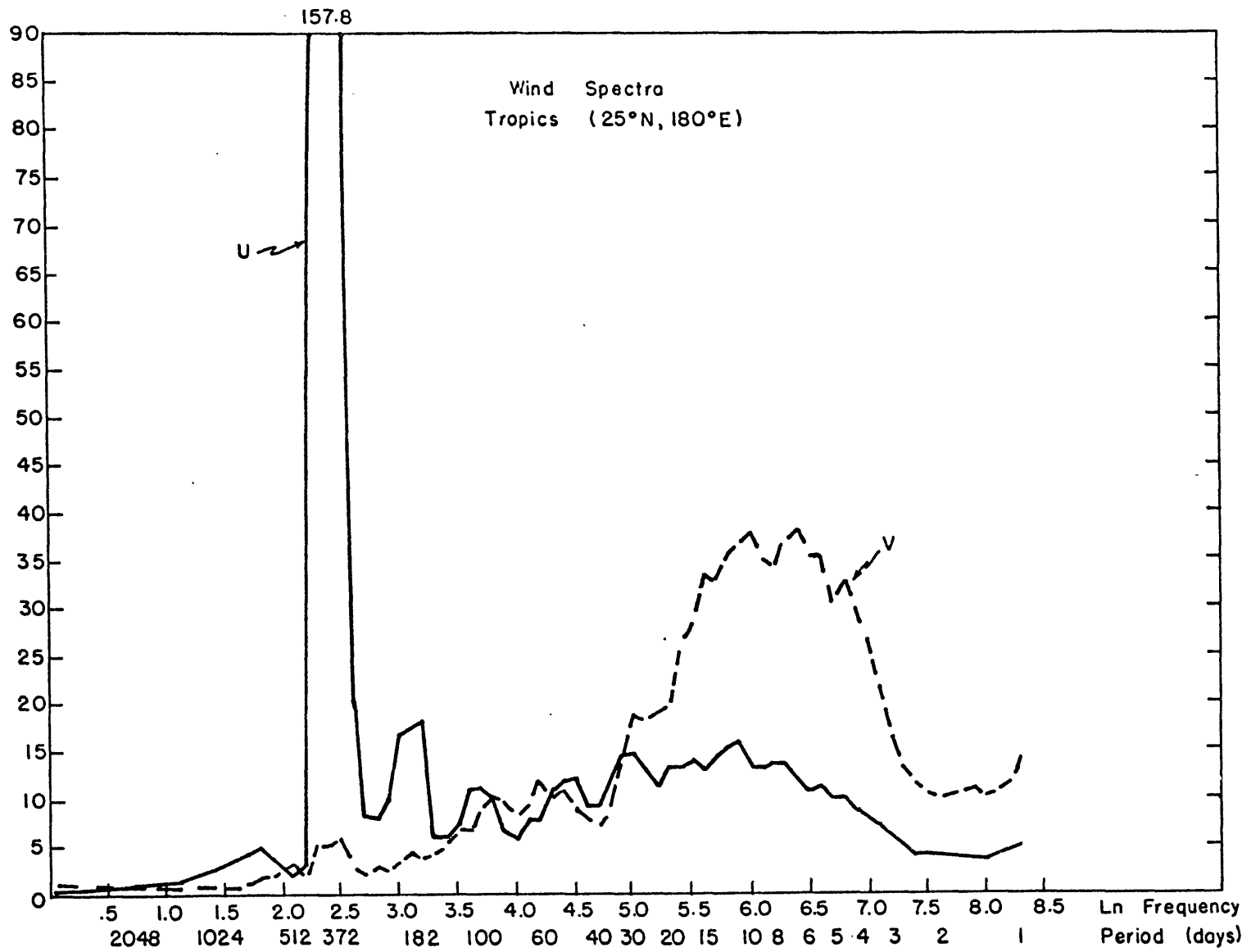


Figure 11.

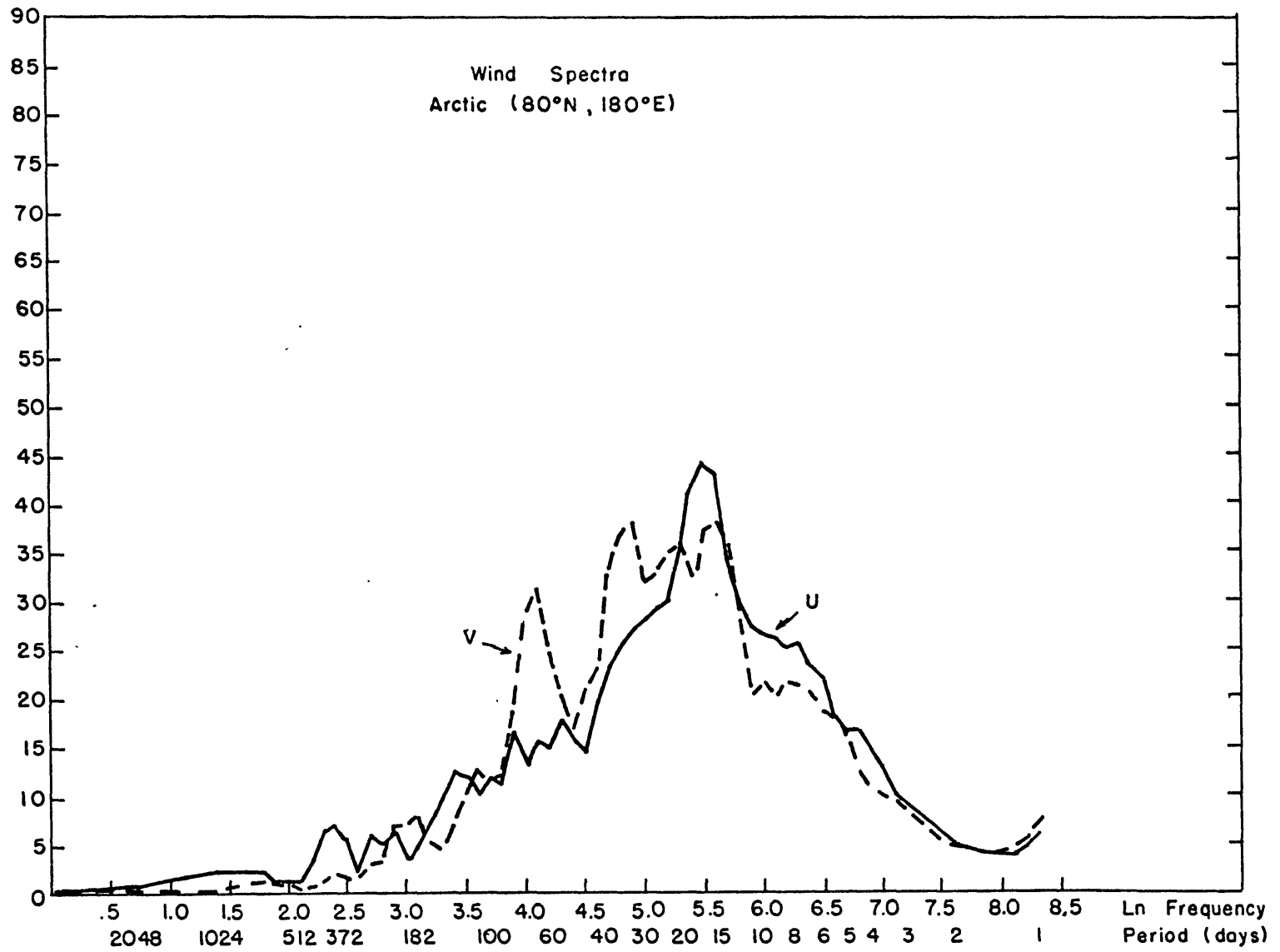


Figure 12.

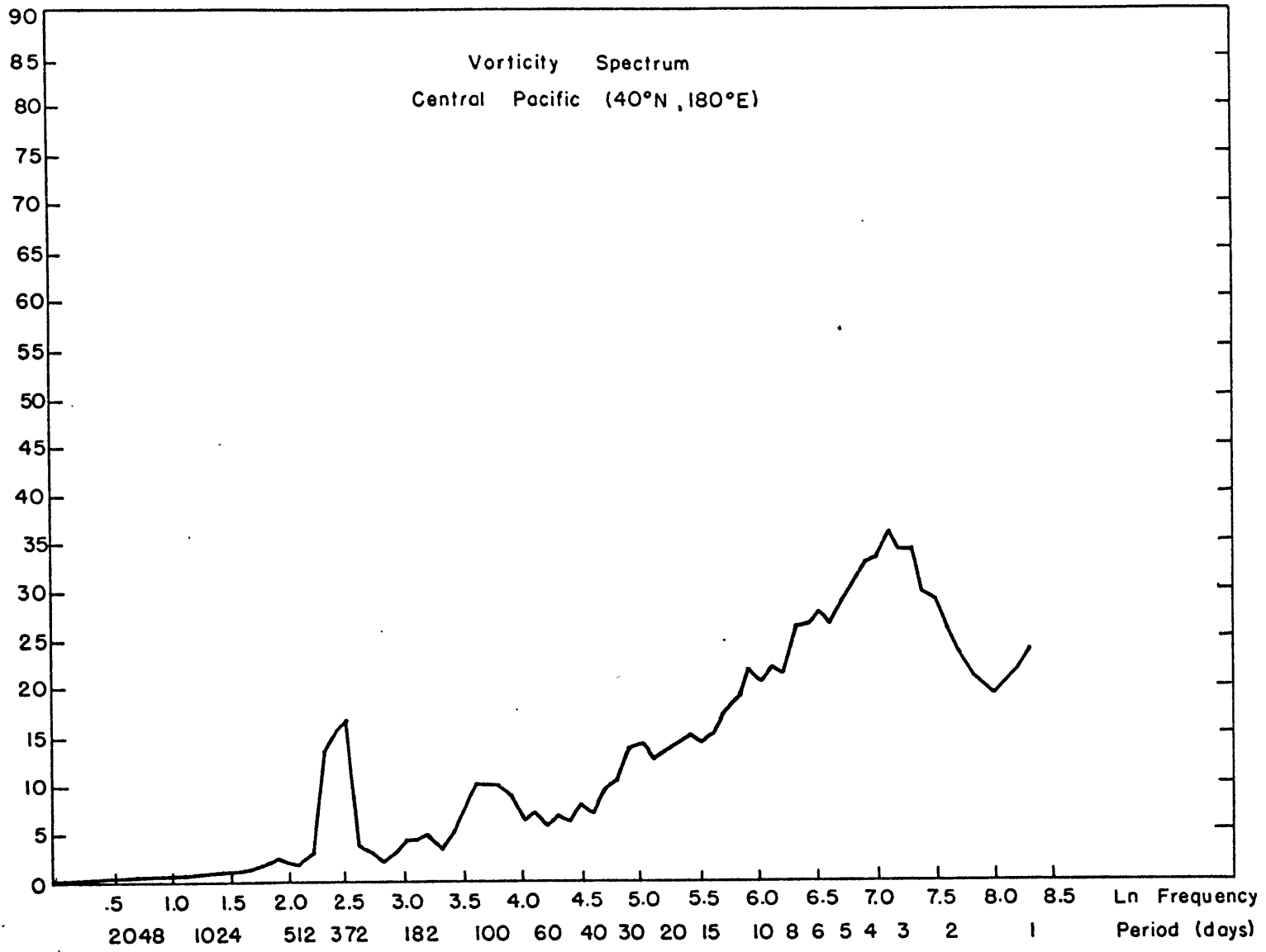


Figure 13.

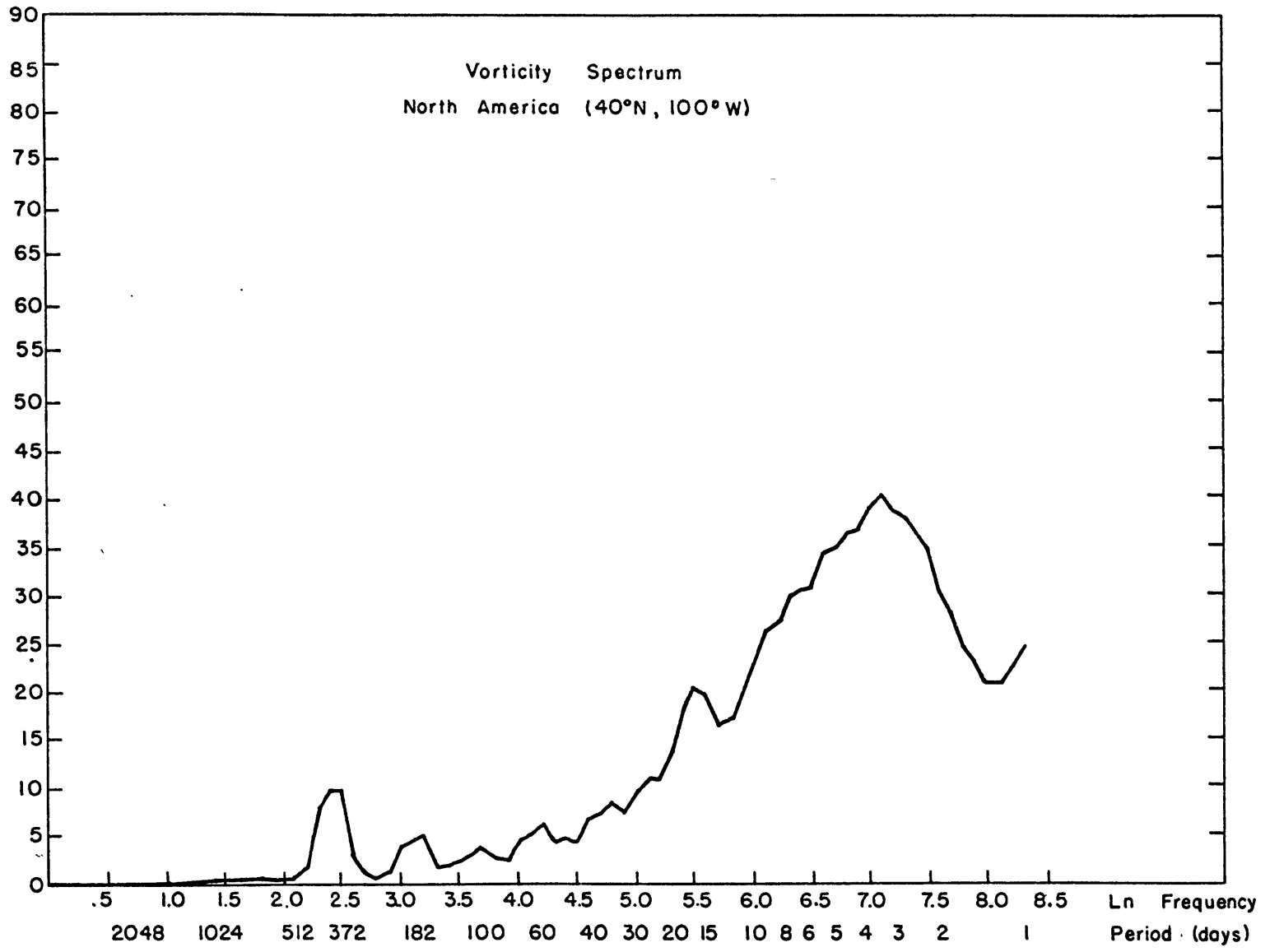


Figure 14.

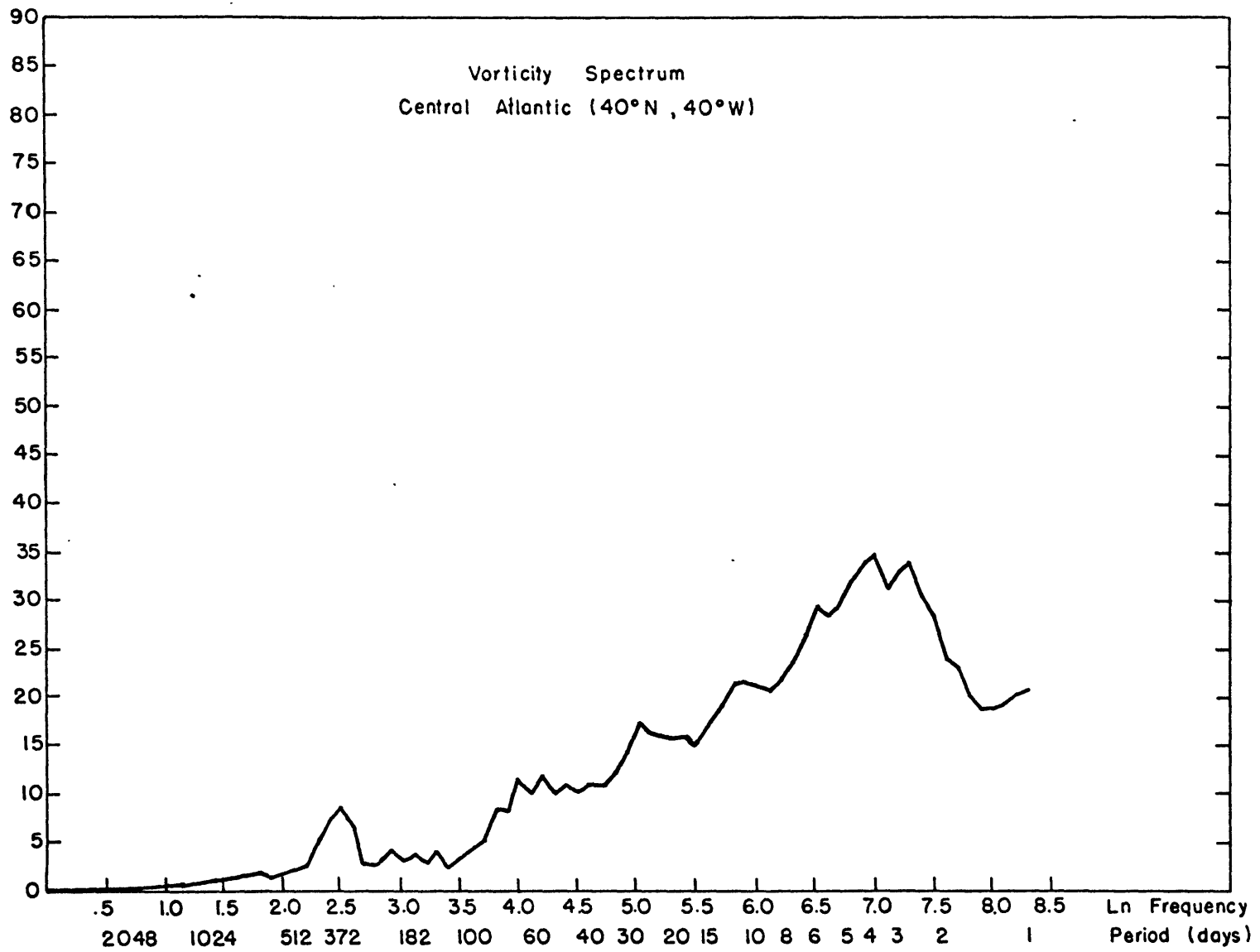


Figure 15.

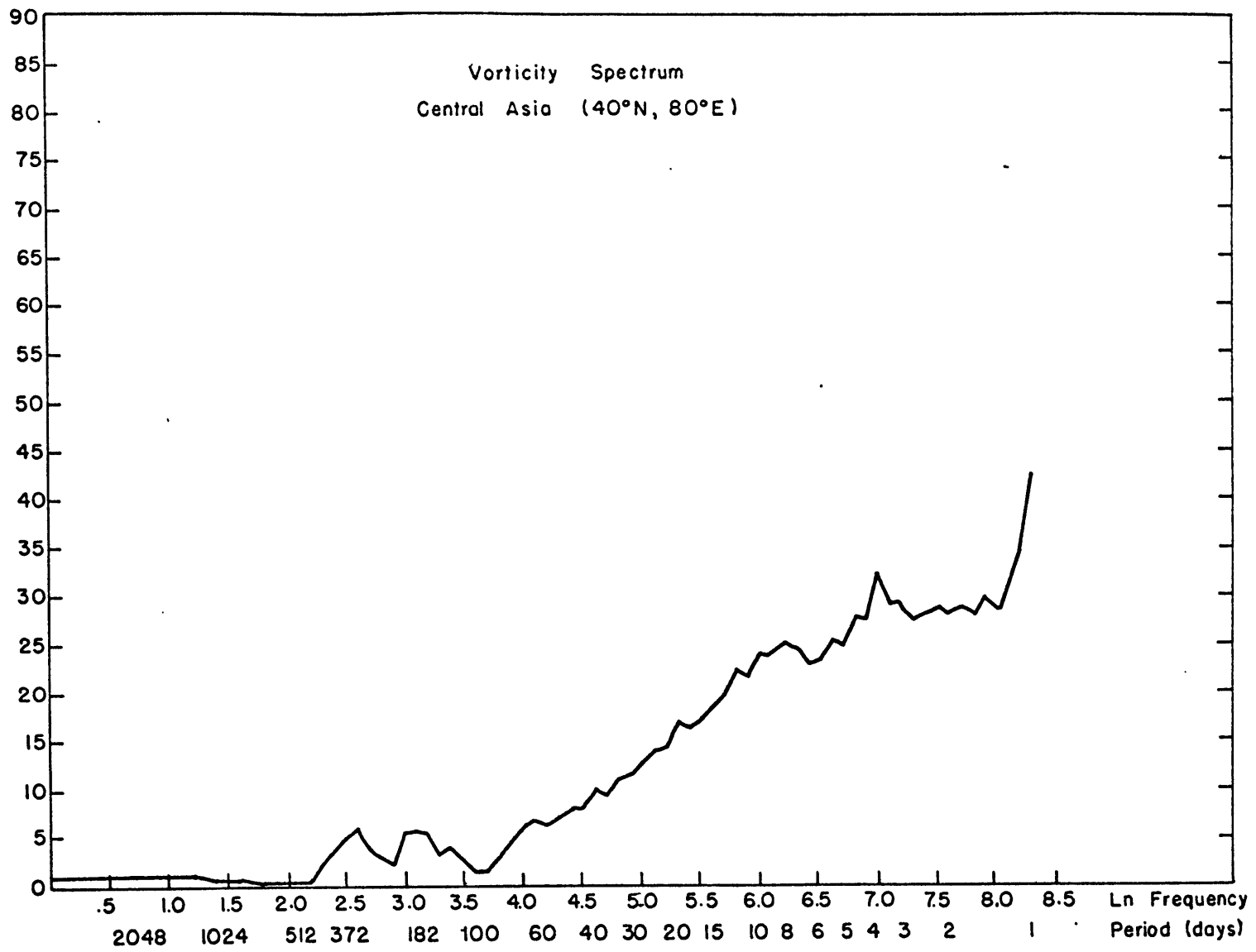


Figure 16.

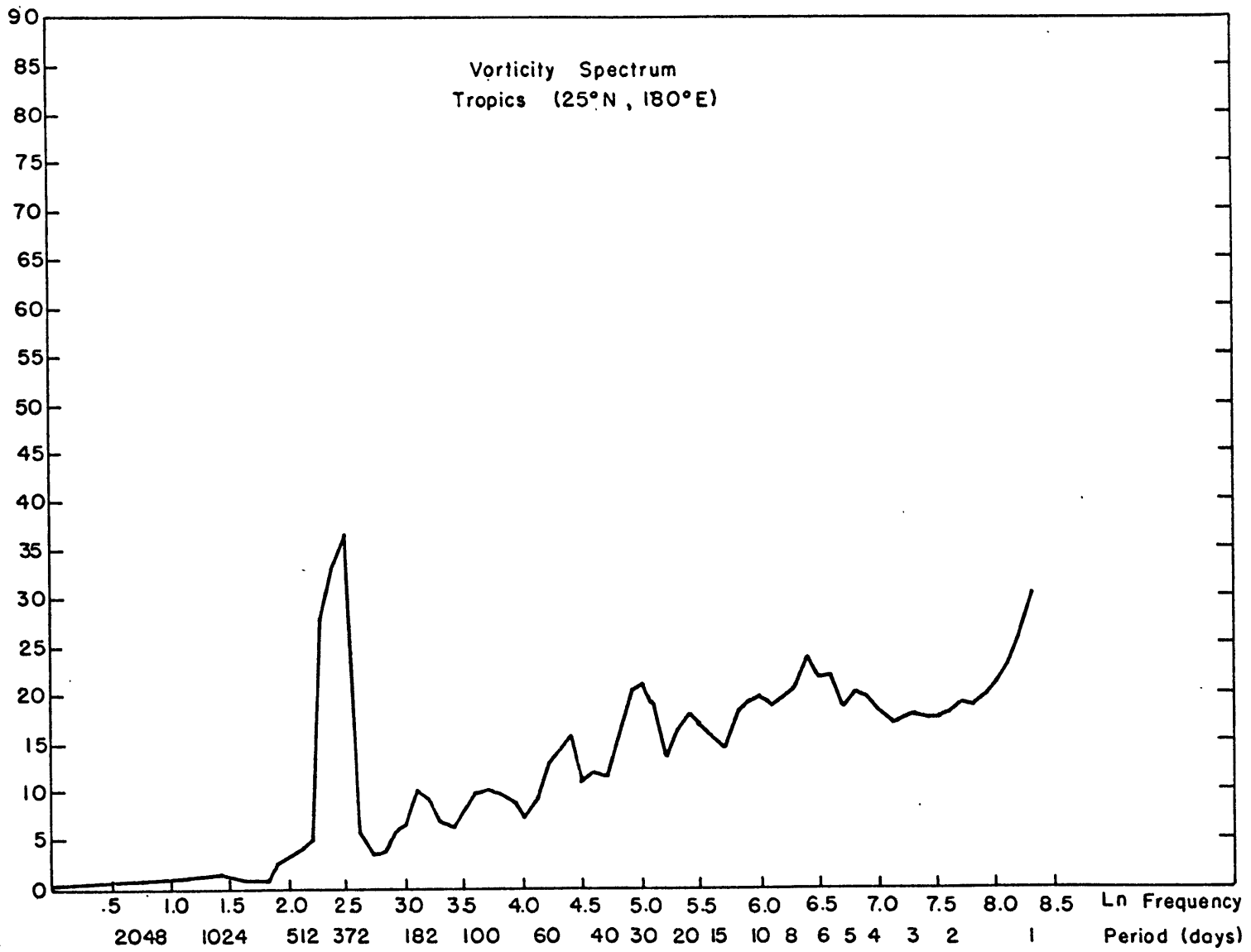


Figure 17.

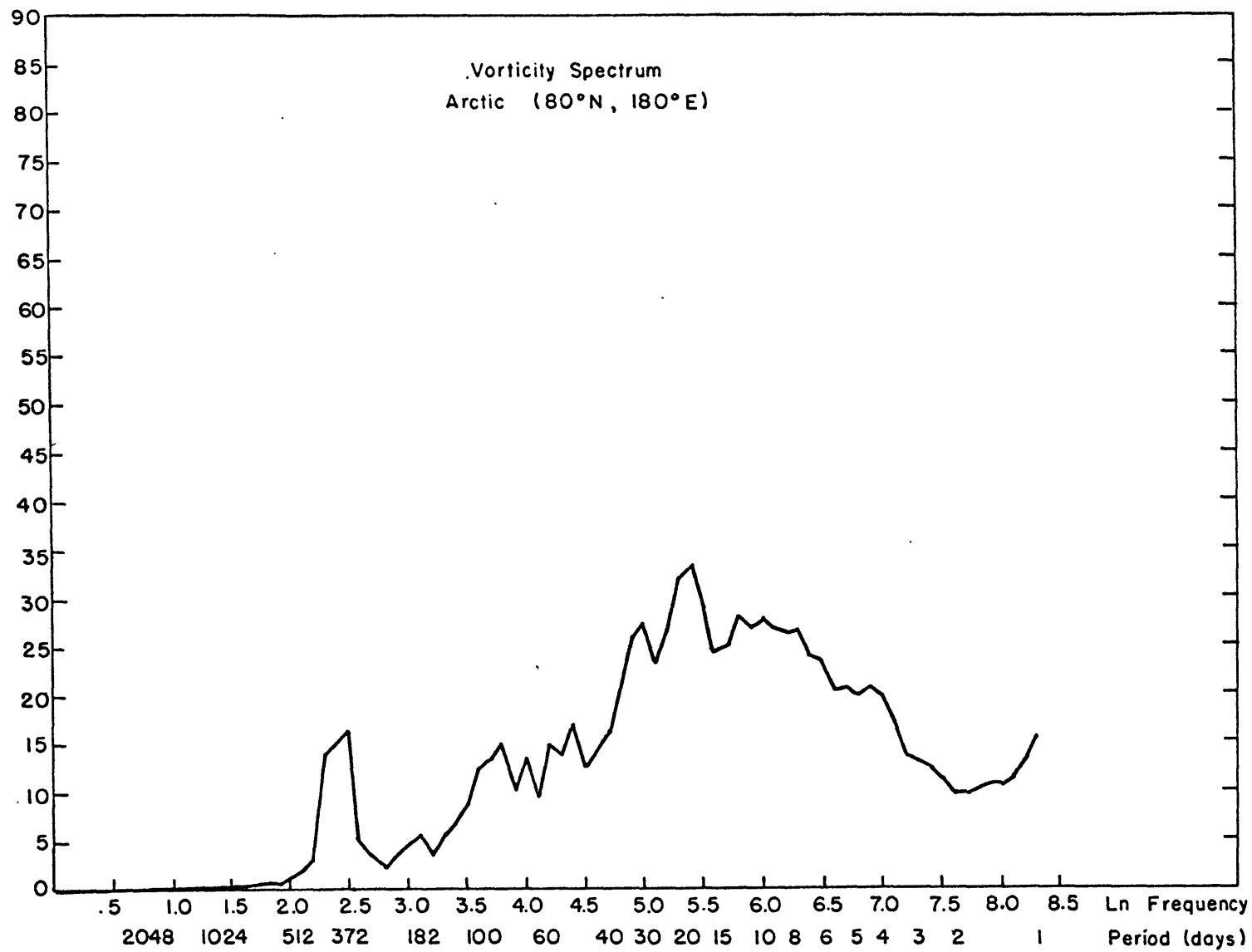


Figure 18.

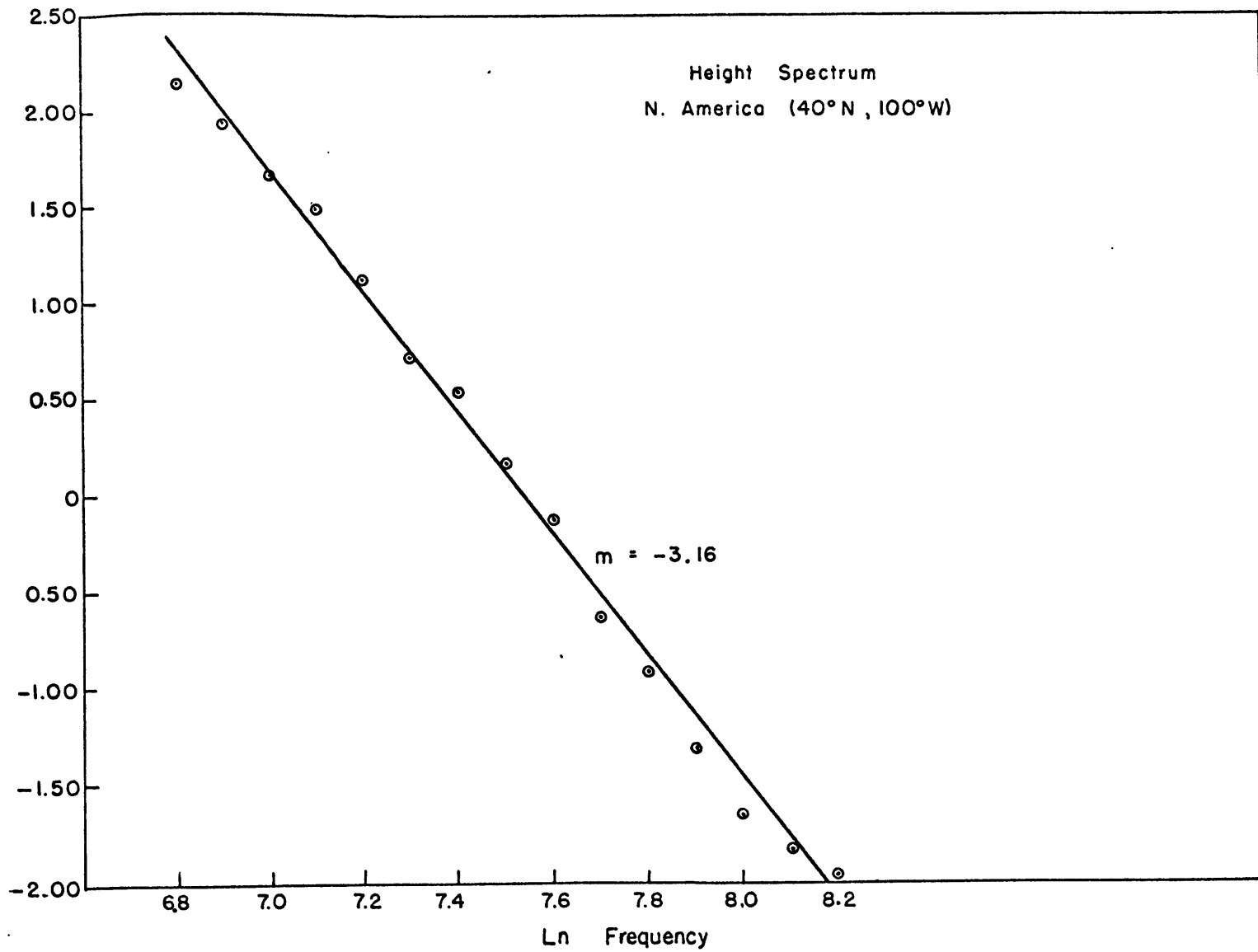


Figure 19.

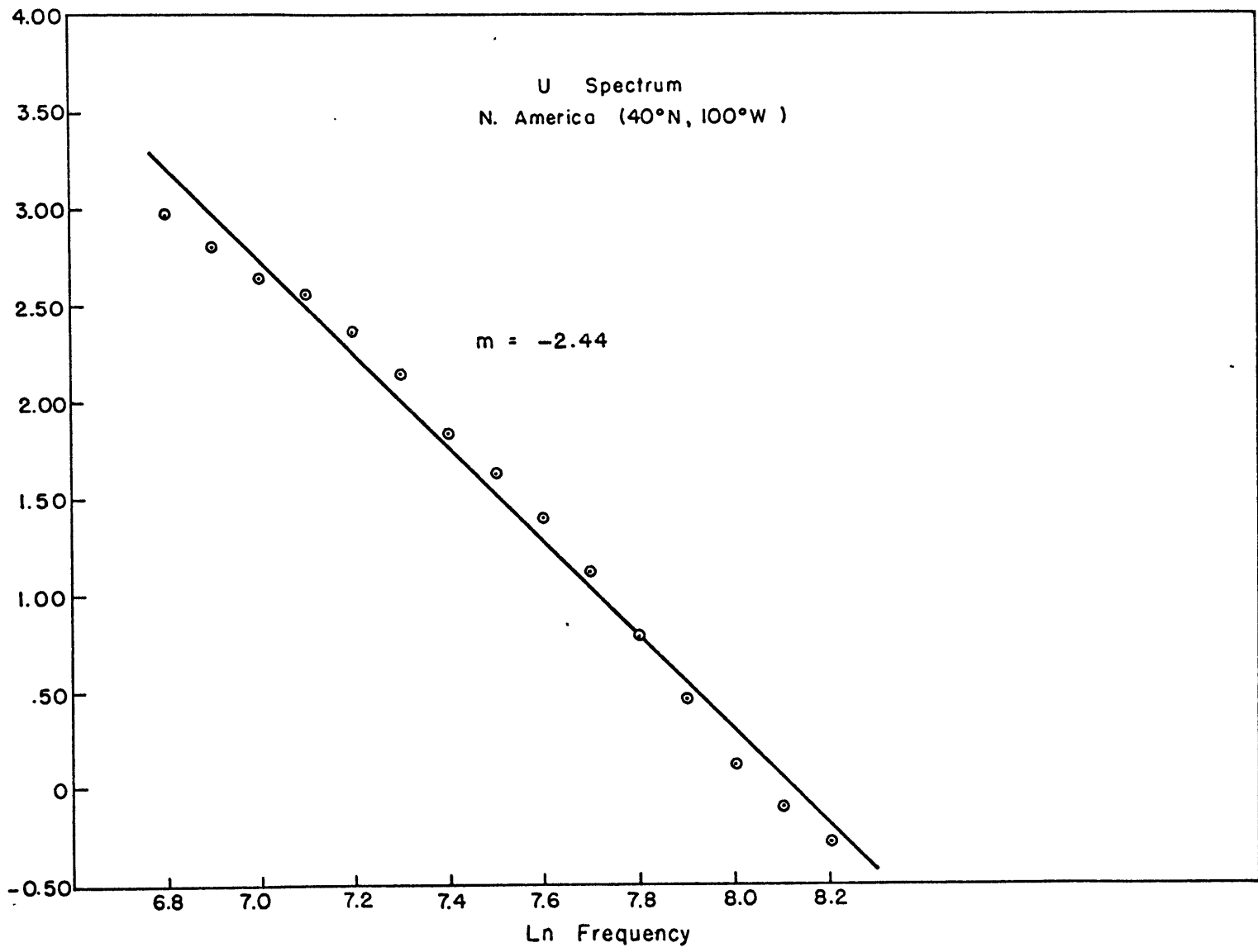


Figure 20.

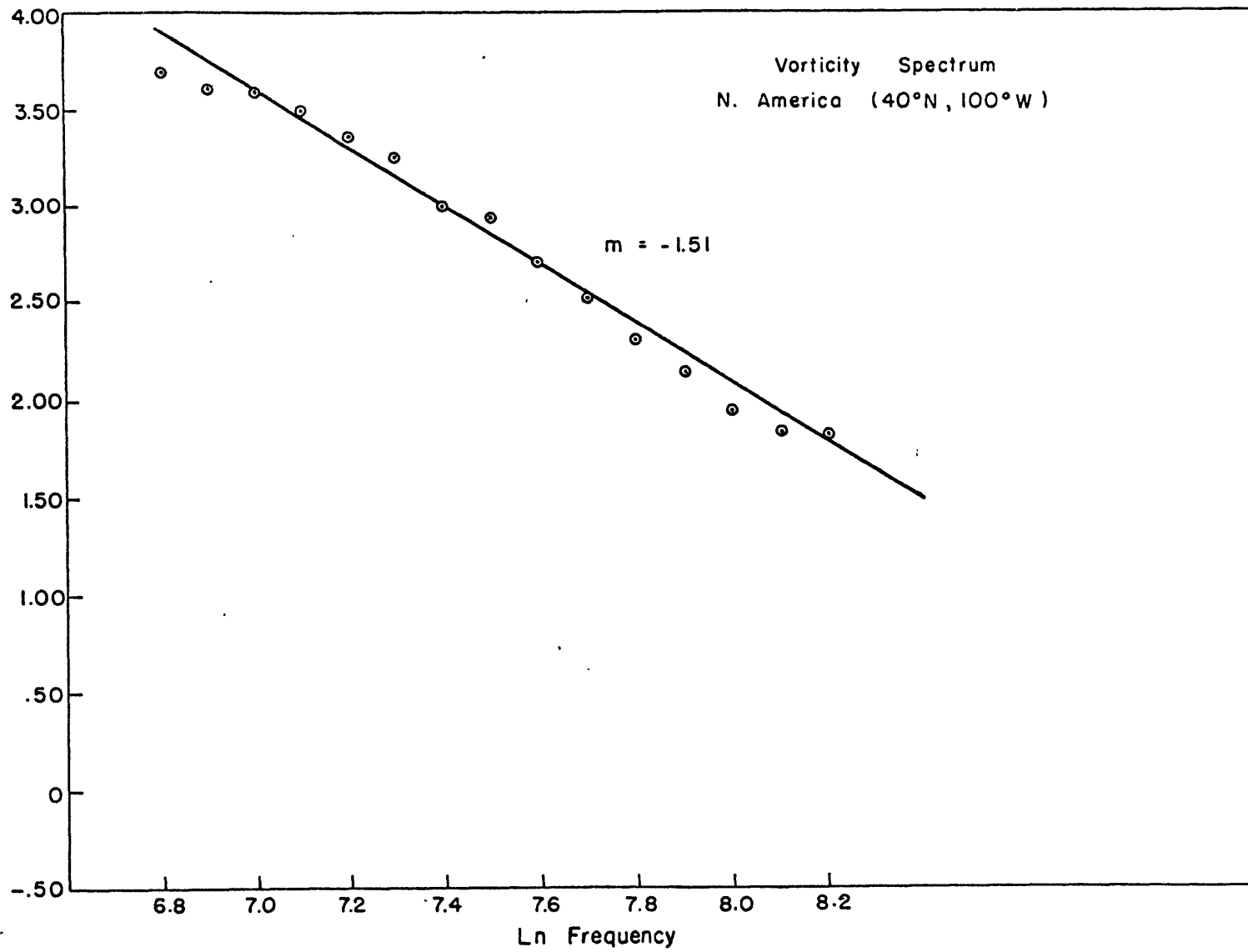


Figure 21.

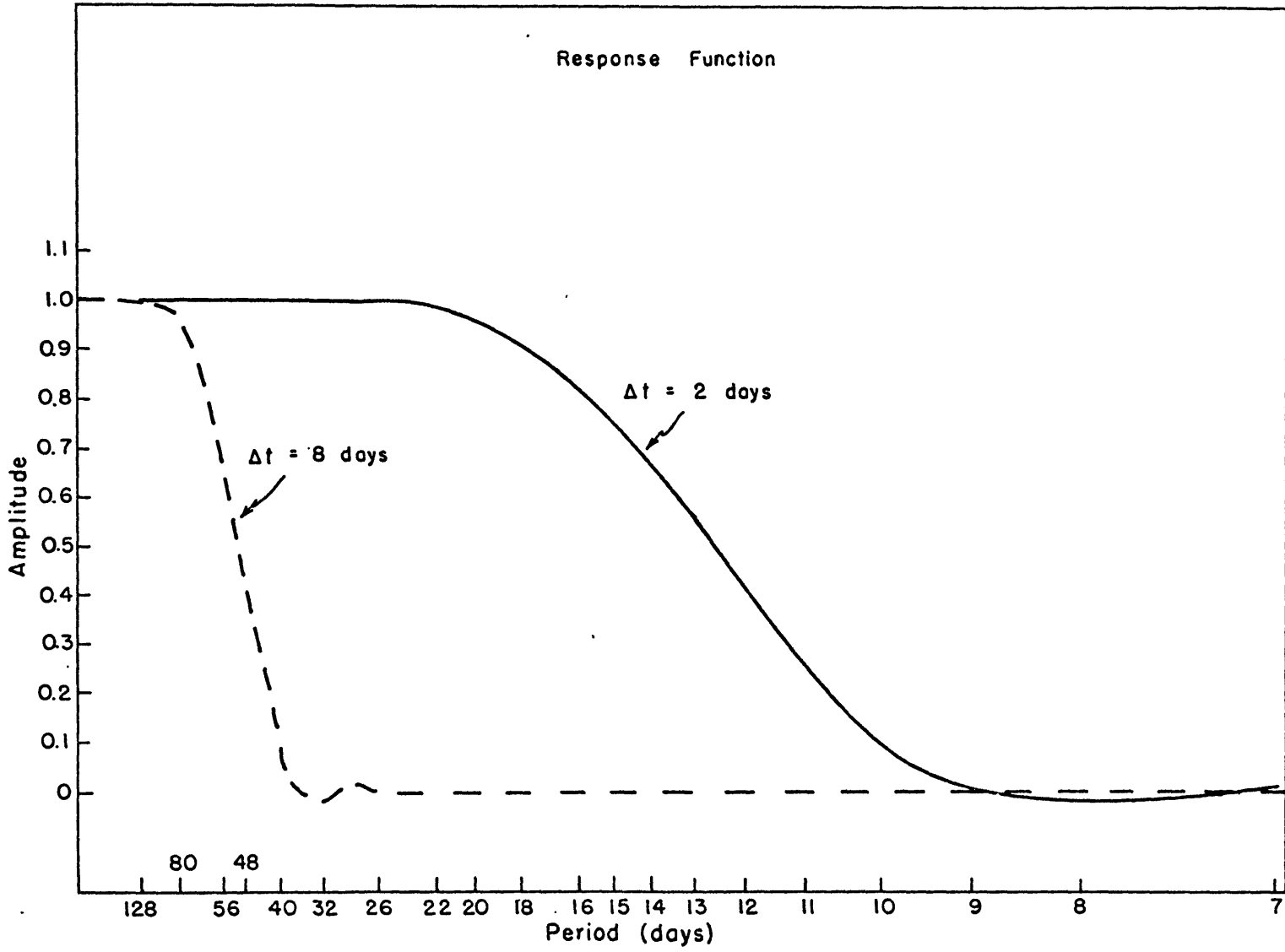


Figure 22.

Finite difference grid for vorticity equation

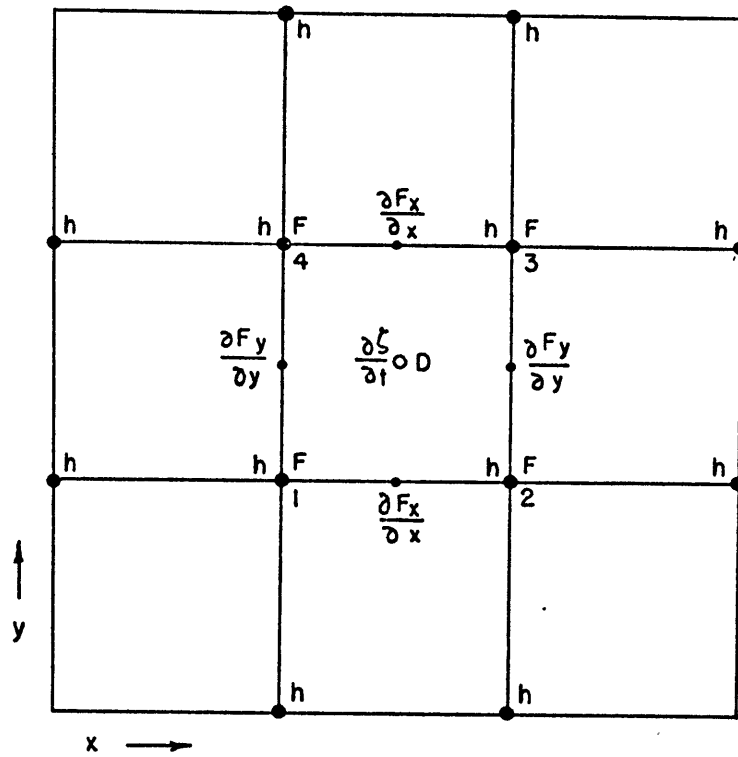


Figure 23.

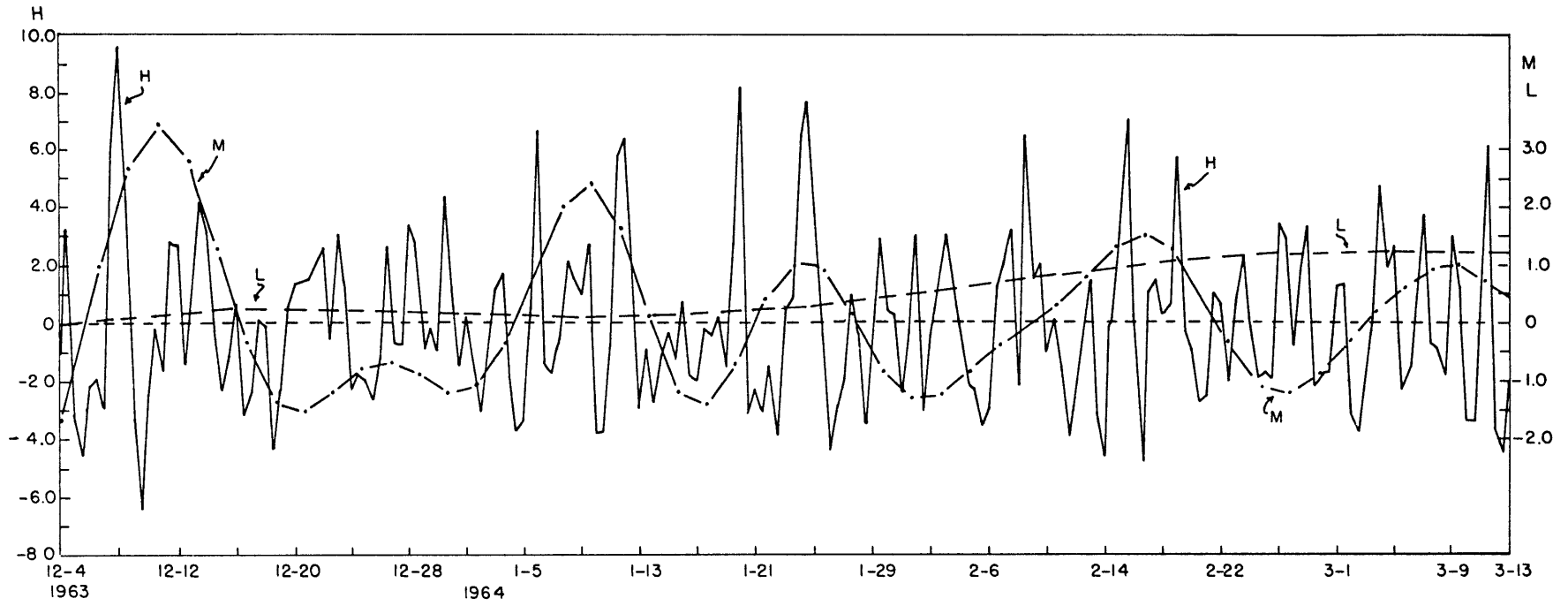


Figure 24.

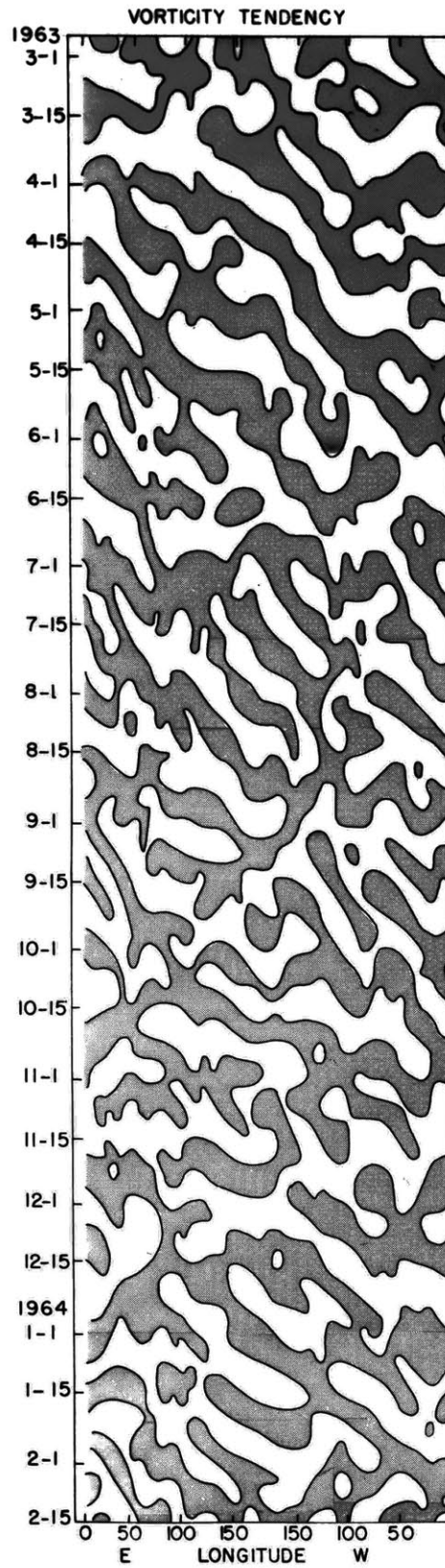
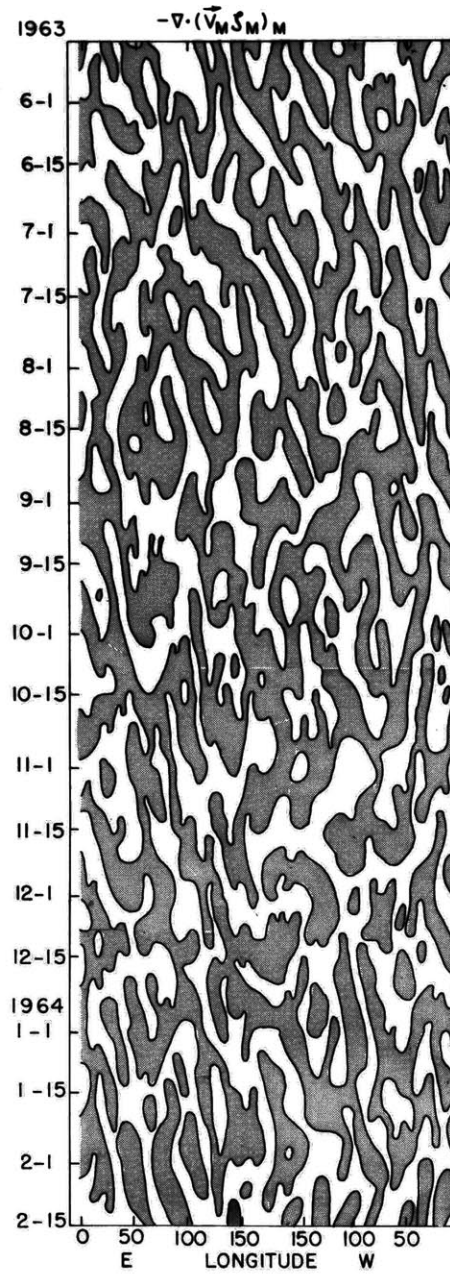


Figure 25.



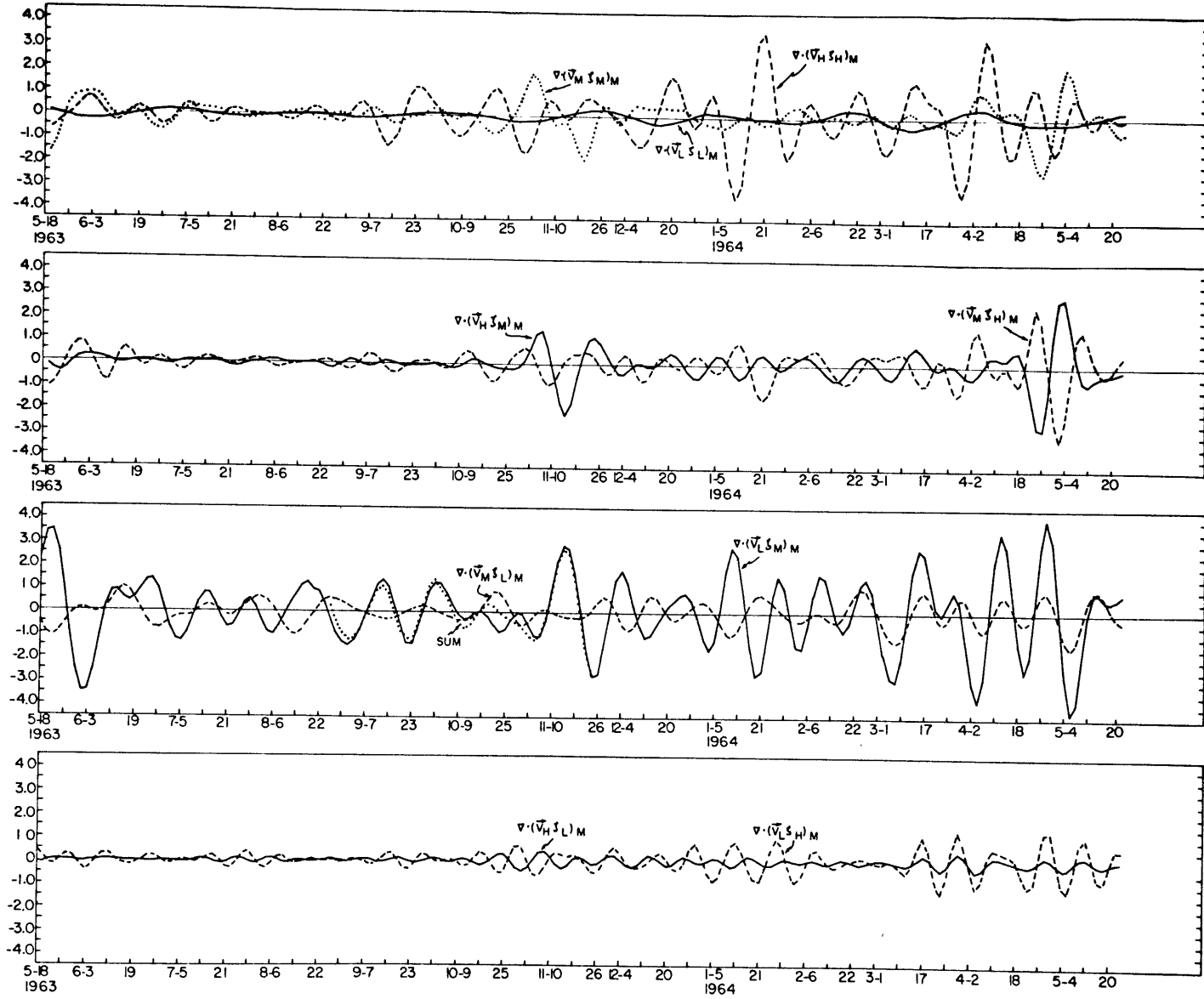


Figure 26a.

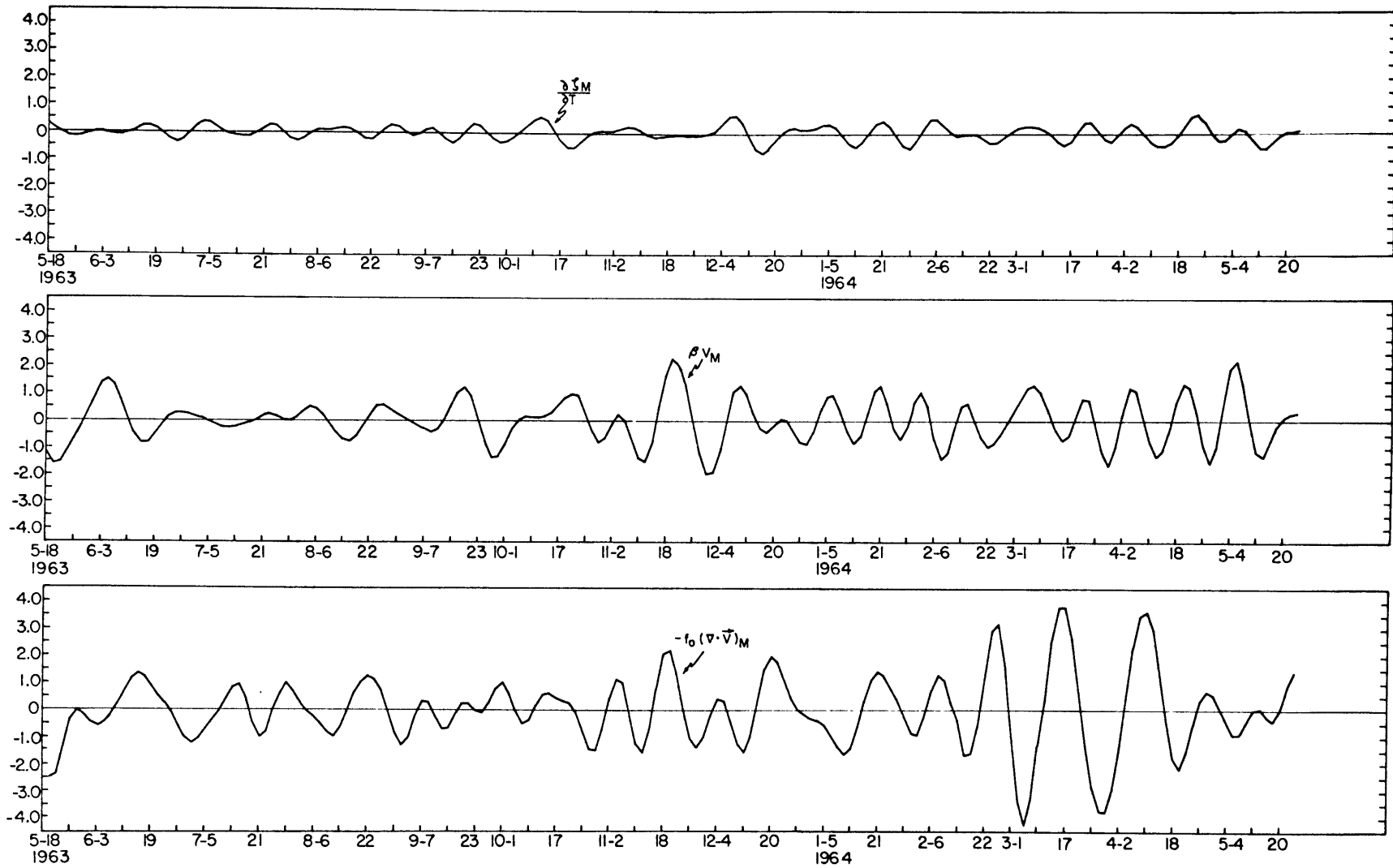


Figure 26b.

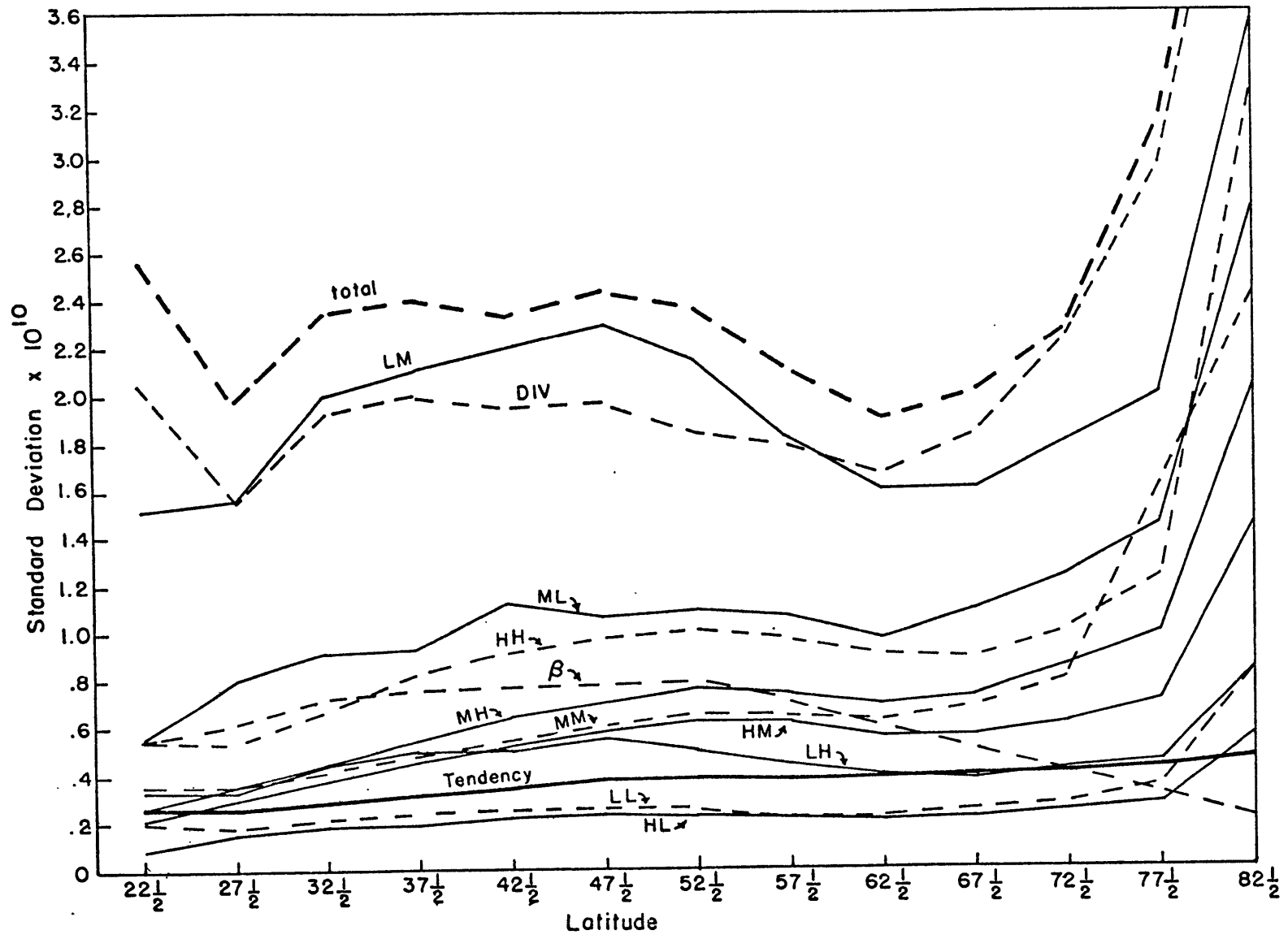


Figure 27.

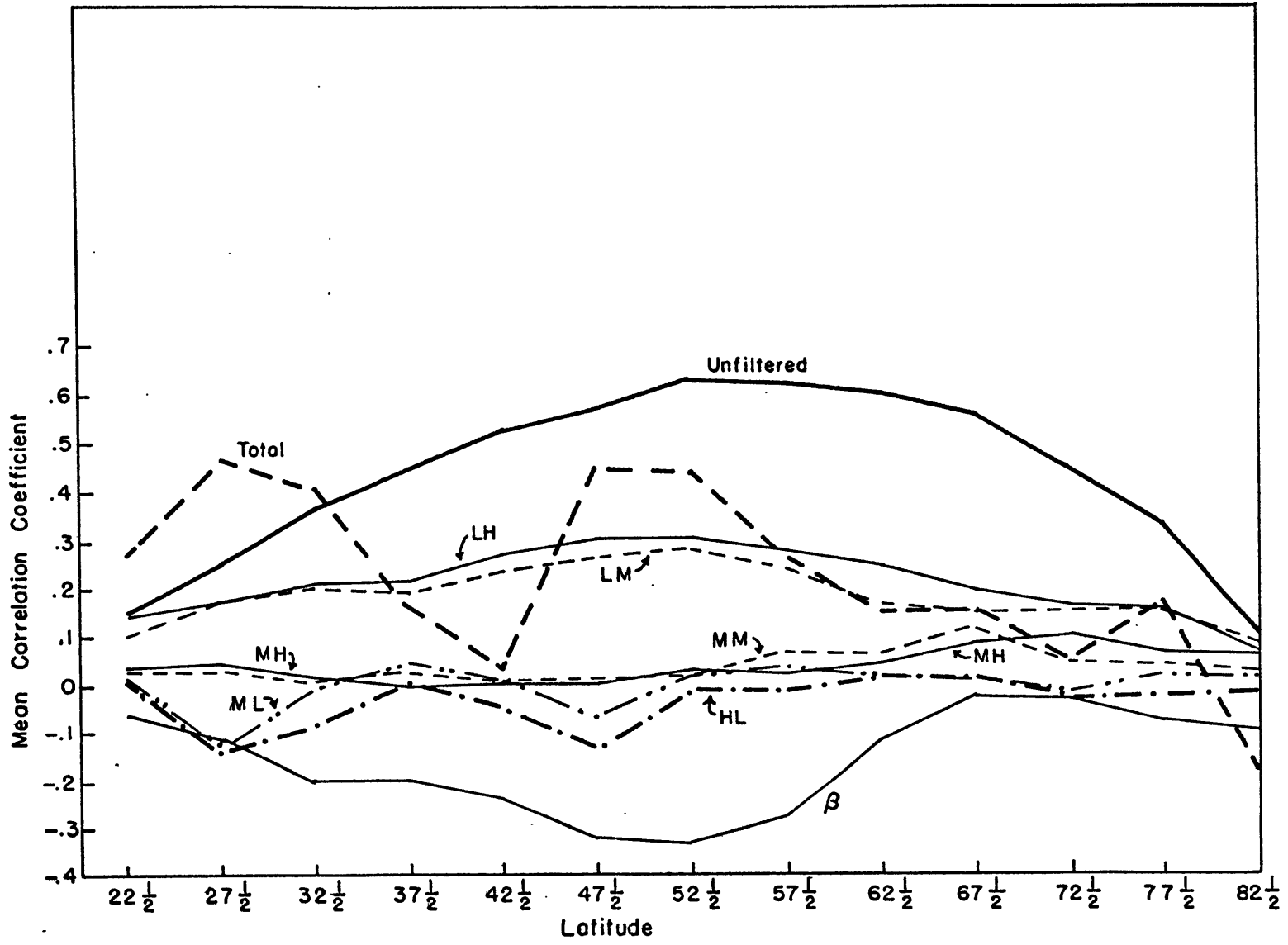


Figure 28.

REFERENCES

- Charney, J.G., 1971, "Geostrophic Turbulence", J. Atmos. Sci., vol.28, pp.1087-1095.
- Chiu, W.-C., 1973, "On the Atmospheric Kinetic Energy Spectrum and Its Estimation at Some Selected Stations", J. Atmos. Sci., vol.30, pp.377-391.
- Clapp, P.F., 1953, "Application of Barotropic Tendency Equation to Medium-Range Forecasting", Tellus, vol.5, pp.80-94.
- Cooley, J.W. and Tukey, J.W., 1965, "An Algorithm for the Machine Calculation of Complex Fourier Series", Mathematics of Computation, vol.19, pp.297-301.
- Deland, R.J., 1965, "Some Observations of the Behavior of Spherical Harmonic Waves", Mon. Weath. Rev., vol.93, pp.307-312.
- Eliassen, E. and Machenhauer, B., 1965, "A Study of the fluctuations of the atmospheric planetary patterns represented by spherical harmonics", Tellus, vol.17, pp.220-238.
- Eliassen, E. and Machenhauer, B., 1969, "On the observed large-scale atmospheric wave motions", Tellus, vol.21, pp.149-166.
- Holloway, J.L. Jr., 1958, "Smoothing and Filtering of Time Series and Space Fields" in Landsberg and Van Miegham (ed.), Advances in Geophysics, New York: Academic Press, vol.4, pp.351-389.
- Holton, J.R., 1972, An Introduction to Dynamic Meteorology, New York: Academic Press, 319 pp.
- Horn, L.H. and Bryson, R.A., 1963, "An Analysis of the Geostrophic Kinetic Energy Spectrum of Large-Scale Atmospheric Turbulence", J. Geophys. Res., vol.68, pp.1059-1064.
- Jenne, R.L., Wallace, J.M., Young, J.A., and Kraus, E.B., 1974, "Observed Long Period Fluctuations in 500 mb Heights: Supplementary Text to NCAR Films J-4 and J-6", NCAR, Boulder, Colo., 65 pp.

- Julian, P.R., 1971, "Some aspects of variance spectra of synoptic scale tropospheric wind components in midlatitudes and in the tropics", *Mon. Weath. Rev.*, vol.99, pp.954-965.
- Julian, P.R., Washington, W.M., Hembree, L., and Ridley, C., 1970, "On the Spectral Distribution of Large-Scale Atmospheric Kinetic Energy", *J. Atmos. Sci.*, vol.27, pp.376-387.
- Kao, S.-K., 1965, "Some aspects of the large-scale turbulence and diffusion in the atmosphere", *Quart. J. R. Met. Soc.*, pp.10-17.
- Kao, S.-K. and Bullock, W.S., 1964, "Lagrangian and Eulerian correlations and energy spectra of geostrophic velocities", *Quart. J. R. Met. Soc.*, pp.166-173.
- Kao, S.-K. and Wendell, L., 1970, "The Kinetic Energy of the Large-Scale Atmospheric Motion in Wavenumber-Frequency Space: I. Northern Hemisphere", *J. Atmos. Sci.*, vol.27, pp.359-375.
- Lahey, J.F., Bryson, R.A., Wahl, E.W., Horn, L.H., Henderson, V.D., 1958, "Atlas of 500-mb Wind Characteristics for the Northern Hemisphere", Univ. of Wisconsin, Madison.
- Lorenz, E.N., 1969, "The predictability of a flow which possesses many scales of motion", *Tellus*, vol.21, pp.289-307.
- Lorenz, E.N., 1973, "On the Existence of Extended Range Predictability", *J. Appl. Met.*, vol.12, pp.543-546.
- Lorenz, E.N., 1974, personal communication.
- Namias, J., 1947, "Extended Forecasting by Mean Circulation Methods", U.S. Weather Bureau, Washington, 89 pp.
- Namias, J., 1953, "Thirty-Day Forecasting: A Review of a Ten-Year Experiment", *Meteorological Monographs*, vol.2, no.6, AMS, Boston, 83 pp.
- Namias, J., 1964, "A 5-Year Experiment in the Preparation of Seasonal Outlooks", *Mon. Weath. Rev.*, vol.92, pp.449-464.
- Oort, A.H. and Taylor, A., 1969, "On the Kinetic Energy Spectrum Near the Ground", *Mon. Weath. Rev.*, vol. 97, pp.623-636.

- Saltzman, B., 1957, "Equations Governing the Energetics of the Larger Scales of Atmospheric Turbulence in the Domain of Wave Number", *J. Meteor.*, vol.14, pp.513-523.
- Saltzman, B. and Fleisher, A., 1962, "Spectral Statistics of the Wind at 500 mb", *J. Atmos. Sci.*, vol.19, pp.195-204.
- Saltzman, B. and Teweles, S., 1964, "Further statistics on the exchange of kinetic energy between harmonic components of the atmospheric flow", *Tellus*, vol.16, pp.432-435.
- Staff Members, Univ. of Stockholm, 1952, "Preliminary Report on the Prognostic Value of Barotropic Models in the Forecasting of 500-mb Height Changes", *Tellus*, vol.4, pp.21-30.
- Steinberg, H.L., Wiin-Nielsen, A., and Yang, C.-H., 1971, "On Nonlinear Cascades in Large-Scale Atmospheric Flow", *J. Geophys. Res.*, vol.76, pp.8629-8640.
- Van der Hoven, I., 1957, "Power spectrum of horizontal wind speed in the frequency range from 0.0007 to 900 cycles per hour", *J. Meteor.*, vol.14, pp.160-164.
- Wiin-Nielsen, A., 1967, "On the annual variation and spectral distribution of atmospheric energy", *Tellus*, vol.19, pp.540-559.
- Wiin-Nielsen, A., Brown, J.A., and Drake, M., 1964, "Further studies of energy exchange between the zonal flow and the eddies", *Tellus*, vol.16, pp.168-180.
- Yang, C.-H., 1967, "Nonlinear Aspects of the Large-Scale Motion in the Atmosphere", Univ. of Mich. Technical Rept. #08759-1-T, 173 pp.
- Young, J.A. and Sikdar, D.N., 1973, "A Filtered View of Fluctuating Cloud Patterns in the Tropical Pacific", *J. Atmos. Sci.*, vol.30, pp.392-407.